

Understanding the Internal Chemical Composition and Physical Processes of the Solar Interior

Sarbani Basu · Nicolas Grevesse · Stephane Mathis ·
Sylvaine Turck-Chièze

Received: 24 May 2013 / Accepted: 20 January 2014 / Published online: 20 February 2014
© Springer Science+Business Media Dordrecht 2014

Abstract The Sun, the closest and most well studied of stars, is generally used as a standard that other stars are compared to. Models of the Sun are constantly tested with helioseismic data. These data allow us to probe the internal structure and dynamics of the Sun. Among the main sources of the data is the SOHO spacecraft that has been continuously observing the Sun for more than a solar cycle. Current solar models, although good, do not include all the physical processes that are present in the Sun. In this chapter we focus on specific inputs to solar models and discuss generally neglected dynamical physical processes whose inclusion could result in models that are much better representatives of the Sun.

Keywords Sun: interior · Sun: helioseismology · Sun: evolution · Sun: abundances

1 Introduction

The Sun is the closest star and hence used as a benchmark to study other stars. In contrast with other stars, its radius, luminosity and mass are known with great accuracy, allowing us

S. Basu (✉)

Department of Astronomy, Yale University, PO Box 208101, New Haven, CT 06520-8101, USA
e-mail: sarbani.basu@yale.edu

N. Grevesse

Centre Spatial de Liège and Institut d’Astrophysique et de Géophysique, Université de Liège,
4031 Angleur-Liège, Belgium
e-mail: Nicolas.Grevesse@ulg.ac.be

S. Mathis

Laboratoire AIM, CEA/DSM-CNRS-Université Paris Diderot, IRFU/SaP Centre de Saclay,
91191 Gif-sur-Yvette, France
e-mail: stephane.mathis@cea.fr

S. Turck-Chièze

SaP/IRFU/CEA CE Saclay, 91191 Gif sur Yvette, France
e-mail: turck-chieze@cea.fr

to make very precise models of the Sun. The current mass of the Sun ($1M_{\odot}$) is estimated to be $1.98892(1 \pm 0.00013) \times 10^{33}$ g (Cohen and Taylor 1987), the radius ($1R_{\odot}$) is $6.9599(1 \pm 0.0001) \times 10^{10}$ cm (Allen 1973), the luminosity ($1L_{\odot}$) is $3.8418(1 \pm 0.004) \times 10^{33}$ ergs s⁻¹ (Fröhlich and Lean 1998; Bahcall et al. 1995). The age of the Sun as determined from radioactive dating of meteorites is $4.57(1 \pm 0.0044)$ Gyr (Bahcall et al. 1995).

One of the more important concepts in modelling the Sun is that of the Standard Solar Model (SSM). The Sun is modelled in a manner somewhat different from other stars since its age, luminosity and radius are known independently. To be called a solar model, a $1M_{\odot}$ model must have a luminosity of $1L_{\odot}$ and a radius of $1R_{\odot}$ at the solar age. The stellar structure equations are solved to satisfy the mass, radius and luminosity constraints. This is done by varying the mixing-length parameter α and the initial helium abundance Y_0 until we get a model with the required characteristics. Mathematically speaking, we have two unknown parameters (α and Y_0) and two constraints (radius and luminosity) at the solar age, and hence this is a well defined problem. The definition of an SSM is somewhat more stringent, with the exception of the mixing-length parameter, the construction of an SSM cannot include any physical quantity or effect that has free parameters in its implementation. Thus for instance SSMs do not include any effects that solar dynamics (rotation, meridional and zonal flows, etc.) may have on solar structure. SSMs are sometimes modified to include a specified amount of convective overshoot, however, since there is no consensus on how overshoot is implemented, this is not common. Just like any other stellar model, an SSM depends on a number of inputs such as radiative opacities, equation of state, nuclear reaction rates, etc. These ingredients have been refined with time as observations from the solar interior (acoustic modes, solar neutrino fluxes) have become more and more accurate. A description of these and other inputs can be found in the review of Turck-Chièze et al. (1993). The observed value of the solar metallicity is also used as a constraint.

SSMs model solar structure very well by the standards of astronomy. For instance, the discrepancy in the sound-speed profile is within a few percent. As helioseismic analyses have shown (see e.g. Christensen-Dalsgaard 2002), the structure of an SSM is in remarkable agreement with the Sun, although the degree of agreement does depend on what we assume the solar metallicity to be. In this chapter we discuss two sources of uncertainty in SSMs—the metallicity, and the equation of state.

The standard solar model, while extremely useful and popular, does not represent all aspects of the Sun. For example, it does not include differential rotation, nor does it include magnetic fields that cause the solar activity cycle and its associated irradiance change (the Schwabe cycle; Schwabe 1844) of about 0.1 % (Fröhlich and Lean 1998). While a 0.1 % change is small, it is still a factor of about 10^5 larger than the change in the luminosity of standard solar models over the same period (Turck-Chièze and Lambert 2007). Without dynamical effects and the effects of magnetic fields one could not hope to model these subtle effects.

In parallel with SSMs, there has also been the development of so-called seismic models of the Sun (see e.g., Antia 1996; Takata and Shibahashi 1998; Turck-Chièze et al. 2001). These are models of the present-day Sun that are forced to satisfy the helioseismic constraints. Some of these are evolutionary models, some others not. For instance the Antia (1996) model is not an evolutionary model, but those of Turck-Chièze et al. (2001) and Couvidat et al. (2003) are evolutionary models obtained by changing opacity and/or reaction rates within their uncertainties. The aim of these models is to predict the thermodynamic properties of the solar core and to estimate neutrino fluxes more accurately. An example of the agreement between the Sun and solar models, one an up-to-date SSM and one seismic, is shown in Fig. 1.

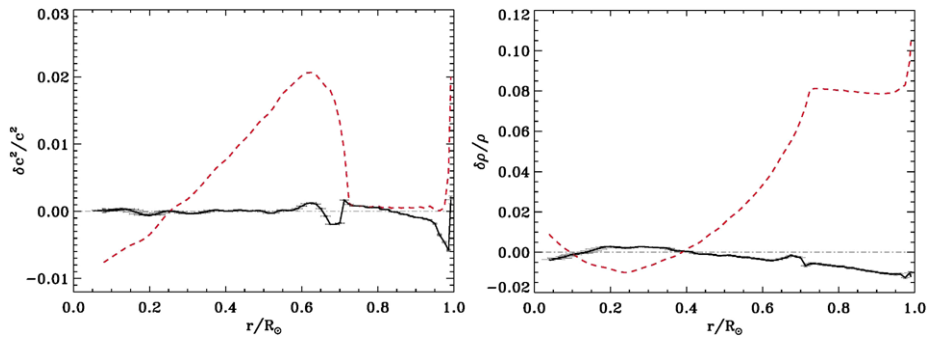


Fig. 1 The difference between the squared sound speed and density profiles of the Sun and two models, one an SSM constructed with Asplund et al. (2009) composition (red dashed lines) and the other the seismic model of Turck-Chièze et al. (2011) (black continuous lines). The errorbars are from the inversion described in Turck-Chièze et al. (2001). See Turck-Chièze et al. (2012) for the list of the values

We have organised this chapter as follows: We first describe the reliability of the data used in determining properties of the solar interior and discuss what we have learned of solar structure thus far. We then discuss the question of solar abundances and describe how the more-recent set of abundances were derived. In the same section we look at the effect of the abundances on SSMs and how they fare in helioseismic tests; we also discuss several attempts that have been made to determine solar metallicity through helioseismic analyses. Next we examine the solar equation of state and review tests of the different equations of state. We then turn our attention to the details of the solar radiative zone and core to discuss what other physics may be needed to model these regions properly. And finally, we discuss angular-momentum transport which is perhaps the most neglected process in solar models.

2 Helioseismic Insights into the Solar Radiative Zone

It is generally believed that SSMs should describe the radiative zone of the Sun reasonably well since, unlike in the convection zone (CZ), dynamical motions are supposed to be negligible in that region. One of the successes of helioseismology has been the ability to determine the structure of the Sun right to the core. MDI (Michelson Doppler Image; Scherrer et al. 1995) and GOLF (Global Oscillations at Low Frequency; Gabriel et al. 1995) are two instruments on board the Solar and Heliospheric Observatory (SoHO) that complement each other. MDI observations have been used to determine solar acoustic-mode frequencies of degree ℓ of 0 to 300. GOLF was built specifically to obtain high-precision data on the solar low-degree modes that allow us to probe the solar core. Combining MDI and GOLF data allows one to determine the sound-speed and density profile of the Sun down to about 0.08 (Basu et al. 2000; Turck-Chièze et al. 2001).

A precise helioseismic description of the solar radiative zone in its entirety presupposes that solar acoustic waves are sensitive to all regions. This however, is not the case. Acoustic modes are by their very nature sensitive to the outer layers of a star because of the lower sound speed (and hence a longer time spent there by the modes) than in the core. They also have higher amplitudes there. Thus even the frequencies of low-degree modes that penetrate deep inside are largely influenced by the outer layers. Easily detectable low-degree modes (i.e., those with frequencies ≥ 2 mHz) contain information of the core (their lower turning points are in that region), however, these modes are also affected by solar-cycle

related changes in the outer layers of the Sun (Gelly et al. 2002; Salabert et al. 2009; Basu et al. 2012; Simoniello et al. 2013). This variability is frequency-dependent, and the change of frequency (up to 0.5 μHz at the maximum of the cycle) is of the same order than the information coming from the core, and thus one needs to correct for this effect or avoid it.

The advantage of GOLF is its very low intrinsic instrumental noise which allows a rapid detection of the lower-frequency part of the spectrum (<1.6 mHz). An extensive discussion of this, as well as a list of the modes, can be found in Turck-Chièze and Lopes (2012). These low-frequency low-degree modes are not visibly affected by magnetic variability in the outer parts of the Sun since the upper turning points of these modes are located below the region that is most affected by magnetic fields. Combining low-degree modes from GOLF with higher-degree MDI frequencies obtained during the solar minimum has led to the determination of sound-speed and density profile in the solar radiative zone down to about 0.08. Results can be found in Basu et al. (2000), where the frequencies that were used were determined using asymmetric Lorentzian profiles for the modes, and Turck-Chièze et al. (2001) where the frequencies had been corrected for magnetic bias. Low frequency acoustic modes are also detectable in ground-based observations collected over decades. Low-degree mode frequencies measured with the Birmingham Solar Oscillation Network (BiSON) when combined with MDI data result in a solar sound-speed profile (see Basu et al. 2009) that agrees with that obtained with the GOLF-MDI combination of data.

The solar sound speed and density profiles are extracted first by determining the sound-speed and density differences between a solar model (the ‘reference model’) and the Sun and then using the known sound speed and density of the model to reconstruct solar values. The sound-speed and density differences are determined from the frequency differences between the model and the Sun, though a correction needs to be applied, commonly known as the ‘surface term’, that accounts for the fact that solar models do not describe the solar near-surface layers correctly. Details of the procedure can be found in Christensen-Dalsgaard (2003). The reference model is usually an SSM. Of course SSMs have evolved because of improvements in input physics, as well as changes in solar composition. Some of these changes have improved the match between SSMs and the Sun, while others have degraded the match. Several groups have regularly constructed and compared SSMs to the Sun. Published SSMs include those of Christensen-Dalsgaard et al. (1996), Bahcall et al. (2001), Turck-Chièze et al. (2001), Christensen-Dalsgaard (2002), Turck-Chièze et al. (2004a), Bahcall et al. (2005), Guzik and Mussack (2010), Turck-Chièze and Couvidat (2011), Turck-Chièze and Lopes (2012), etc.

In Fig. 2, we show a detailed view of sound-speed and density in the solar core. The results, with corresponding uncertainties, can be found in Turck-Chièze and Lopes (2012). The details of the difference between the Sun and the models depend on the data used and of course the model, but most groups agree that there are statistically significant difference between the Sun and models throughout the radiative zone. Thus it can be reasonably assumed that SSMs match the Sun only to a few percent. The precision of the seismic probes is such that it impels us to determine the origin of these discrepancies that are small, but statistically significant.

3 The Issue of Solar Abundances

The heavy-element mass fraction (i.e. mass fraction of elements heavier than helium), Z , of the Sun is one of the fundamental inputs to solar models. Z affects energy transport

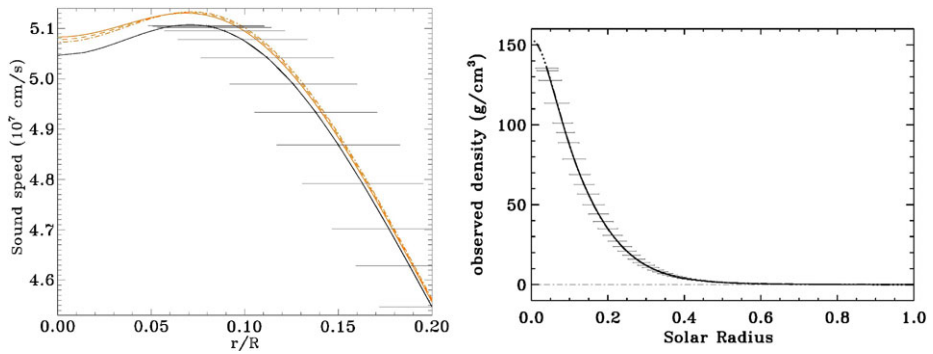


Fig. 2 The sound speed in the solar core, and density in the radiative zone. Note the better agreement with a seismic solar model in *black* (the *vertical errorbars* on the points are too small to be visible) than with the SSM or with the solar model with modified energy production (*red*), see Turck-Chièze et al. (2011) for details. The *horizontal errorbars* are a measure of the resolution of the inversions and denote the width of the resolution kernels

through its effect on radiative opacities. The abundance of some specific elements, such as oxygen, carbon, and nitrogen, can also affect the energy generation rates through the CNO cycle. The effect of Z on opacities changes the boundary between the radiative and convective zones, as well as the structure of radiative region; the effect of Z on energy generation rates can change the structure of the core. Although, the main effect of heavy element abundances is through opacity, these abundances also affect the equation of state. In particular, the adiabatic index Γ_1 is affected in regions where these elements undergo ionisation. The importance of the solar heavy-element abundance does not merely lie in being able to model the Sun correctly, it is often used as the standard against which heavy-element abundances of other stars are measured. Thus the predicted structure of those stars too become uncertain if the solar heavy-element abundance is uncertain. As analysis techniques have changed, there have been related changes in the solar heavy element abundance.

A decrease by 30 % of the photospheric iron abundance that was announced in the 1990s had deteriorated, slightly, the agreement between the sound-speed profile obtained from helioseismic analyses and that of solar models (Turck-Chièze and Lopes 1993). Indeed until about 2002, the reported abundances were such that solar models constructed with those abundances matched the structure of the Sun to an amazing degree (see e.g., Turck-Chièze et al. 2001; Christensen-Dalsgaard 2002; Basu and Antia 2008, and references therein). Since then however, there has been a steady decrease in the reported value of solar metallicity, and this has resulted in models that do not agree with the Sun (see e.g., Basu and Antia 2004, 2008; Bahcall et al. 2005; Turck-Chièze et al. 2004a, and references therein). While lower abundances, particularly lower oxygen abundance, have led to models that do not agree with the Sun, the lower solar abundances, if correct, also mean that the solar oxygen abundance is no longer higher than that of other nearby stars (Turck-Chièze et al. 2004a). Some of the authors of this chapter have been involved on opposite sides of this debate; thus we present below a detailed view of both why the new abundances are considered better than the old ones (Sect. 3.1) and what helioseismic analysis tells us about the newer heavy-element abundance determinations and that helioseismic analyses generally yield higher Z (Sect. 3.2).

3.1 Determining Solar Abundances

When one examines the evolution of the solar chemical composition during the last two decades, looking at different reviews, one sees that the progress has, essentially, been due to progress in the accuracy of the atomic data, mostly the transition probabilities. The resulting changes in Z were small. The situation has, however, changed recently with the rather severe downward revisions of the abundances of a few elements. The new analyses of the solar chemical composition are summarised in the reviews by Asplund et al. (2009), Caffau et al. (2011, see also the references in those two reviews). The new photospheric results are significantly smaller for the most abundant elements like C, N, O, and Ne than those recommended in the widely used compilations of Anders and Grevesse (1989), Grevesse and Noels (1993) and Grevesse and Sauval (1998). They are generally only somewhat smaller for the other elements. As the solar metallicity is essentially dominated by oxygen (43 %), carbon (18 %), neon (10 %), and iron (10 %), the older metallicities from these three compilations, from $Z = 0.02$ to $Z = 0.017$ (iron reduction), decrease to $Z = 0.0134$ with the new solar mixture of Asplund et al. (2009).

We briefly review the changes of the last 15 years and discuss the main reasons for the downward revisions of the abundances of the important elements like O, C and Ne.

3.1.1 *The New Analysis*

Asplund et al. (2009) re-determined the abundances of nearly all available elements. The authors used a new 3D hydro-dynamical solar model atmosphere instead of the classical 1D models of the photosphere used for many decades. They did a careful and demanding selection of the spectral lines and when possible, replaced the often used LTE hypothesis by non-LTE analyses. In the cases of C, N and O, they used many different indicators of the abundances, atoms as well as molecules. From the available atomic and molecular data, they only used those that they considered to be the most reliable. These points are discussed below, along with the solar spectra that are the basis of all the analyses.

3.1.2 *Solar Spectra*

The most commonly used optical disk-center intensity spectra of the quiet Sun are the so-called Jungfraujoch or Liège atlas (Delbouille et al. 1973, after its locations of observation and production, respectively) and the Kitt Peak solar atlas (Neckel and Labs 1984). The spectral resolution of the latter is slightly higher, whereas the former is less affected by telluric absorption owing to the much higher observing altitude. There are also corresponding IR disk-center intensity atlases observed from Kitt Peak (Delbouille et al. 1981) and from the Atmospheric Trace Molecule Spectroscopy (ATMOS) experiment flown on the space shuttle (Farmer and Norton 1989; Abrams et al. 1996), as well as from the recent ACE spacecraft experiment (Hase et al. 2010). In the new analyses, although excellent quality solar flux spectra were available, the authors avoided using such spectra because the lines are formed higher in the atmosphere, in regions that are more sensitive to departures from LTE that are still difficult to estimate in many cases. When possible, they also avoided using lines in the blue or near UV, because the density of spectral lines per unit wavelength in these spectral regions is very large, and the probability of unknown blends therefore very high. All solar atlases agree very well with each other except for spectral regions afflicted by telluric features. Thus, the quality of observations is in general not a source of significant error in solar abundance analyses.

3.1.3 Solar Photospheric Models

The new analyses of the solar chemical composition (Asplund et al. 2009; Caffau et al. 2011, see also the references in these two reviews) were driven by the availability of three-dimensional (3D), time-dependent, hydrodynamical models of the solar atmosphere that were successfully applied to the solar spectrum line formation. Various classical 1D models of the photosphere are also used for comparison. The empirical model of Holweger and Mueller (1974) has been used in a large number of solar abundance analyses since more than 30 years. In addition, Asplund et al. (2009) applied theoretical models like MARCS (Gustafsson et al. 2008) and Kurucz (see <http://kurucz.harvard.edu>). In stellar abundance analyses, such models are often used. When comparing stellar and solar results, data have to be obtained with the same type of model since abundances might be very model-dependent. They also used a mean 3D model, 1DAV (1D averaged) that is a result of temporally and horizontally averaging the 3D model mentioned on surfaces of equal optical depths. Comparing 3D and 1DAV results, actually shows the role played by the heterogeneities.

Details of the main characteristics of the 3D models can be found in Stein and Nordlund (1998) and Nordlund et al. (2009). To summarise, the models successfully reproduce a wide range of observational constraints. The observed heterogeneous and ever changing nature of the photospheric granulation is successfully modelled. These 3D models have enough realistic physics that allow one to reproduce the solar line profiles as they are really observed in the solar spectrum: all the line profiles are asymmetric, the bisectors of the unblended lines show a delicate C-shape, and the wavelength of the centres of the lines are shifted to the blue. These subtle characteristics in the shapes of the lines result from the motions of matter in the photosphere caused by convective-overshoot from the solar convection-zone into the photosphere. 1D models cannot reproduce these subtle but important properties of the line profiles, leading to unshifted, symmetric lines. Furthermore, the widths of the spectral lines are predicted naturally with the 3D models without invoking any fudge parameters like micro- and macro-turbulence needed with 1D models. The new generation of 3D models reproduce in detail the observed centre-to-limb variation of the continuous intensity and the absolute intensity.

3.1.4 Selection of the Lines, Non LTE-Molecules

Asplund et al. (2009) selected lines keeping in mind that inclusion of blended lines increases the abundance scatter and skews the results towards erroneous larger abundances. Thus the shape of each line profile was compared to the ideal shape computed with the 3D model. This resulted in discarding a number of good candidates that did not show obvious traces of blends, but that were probably slightly blended since their shape do not obey the C-shape rule. It was also found that many lines do not obey the local thermodynamic equilibrium (LTE). Non-LTE analyses were done when possible i.e. when the atomic data were available. Generally missing are accurate values for the cross-sections of the collisions with the neutral hydrogen atoms. This is the main source of uncertainty for lines that show large non-LTE corrections. To determine the abundances of C, N and O, molecular lines of CH, C₂, CO, CN, NH and OH were used. Many of these lines (except for C₂) are in the IR where they are not blended at all. For these elements, the molecular lines are better indicators of the abundances, than the high-excitation lower levels of the atoms, since there is more C, N and O in molecules.

3.1.5 Differences Between New and Old Solar Mixtures

The largest downward revisions that occur for the most important elements, O and C are discussed below. Also discussed is the abundance of Ne, since the solar Ne abundance is derived from the Ne/O ratio that can only be measured in the corona.

Both O and C have low excitation forbidden lines and very high excitation permitted lines (O I and C I) as well as a large number of very good molecular lines. In the old solar mixtures of Anders and Grevesse (1989), Grevesse and Noels (1993) and Grevesse and Sauval (1998), as well as in the new one of Asplund et al. (2009) the abundances of O and C are determined from these indicators. However, in the old analyses, the solar photospheric model was the popularly used 1D model of Holweger and Mueller (1974), and the LTE hypothesis was also adopted. The solar data were essentially the same as the ones used nowadays. The main characteristics of the results of the three older analyses are the following: the results from the various indicators, permitted and forbidden atomic lines and molecular lines, agree within about 0.1 dex, leading to abundances of O between 8.8 and 8.9 (the abundances are given in the usual logarithmic astronomical scale relative to hydrogen, where $\log N(\text{H}) = 12$) and the evolution from 1989 to 1998 is essentially due to progress in the atomic and molecular data used to derive the abundances. The differences between the new, 8.69 (Asplund et al. 2009) and old oxygen abundance, 8.83 (Grevesse and Sauval 1998, as mentioned in the review presented in Vol. 5 of the Space Sciences Series of ISSI) can be explained as follows. The decrease of the abundances derived from the three forbidden lines is due to the presence of blends unknown 15 years ago. The authors estimated the importance of these blends in a purely empirical way independent of any model atmosphere. The results from these forbidden lines are not sensitive to any non-LTE effects nor to the model. The decrease of the abundance derived from the very high excitation permitted O I lines is due to departures from LTE affecting those lines. These non-LTE effects could not be computed 15 years ago because of the lack of the required atomic data. The decrease of the abundance from the molecular lines is the result of the new 3D model—the mean temperature of the 1D model used 15 years ago (Holweger and Mueller 1974), is a bit too high in the somewhat higher layers where the molecular lines are formed, leading to anomalously large abundances. The new final abundances from the 3 different indicators are in agreement, the differences being less than 0.01 dex. The old values also agreed but with a larger scatter, of order 0.1 dex, between the various indicators. The situation for C is very similar to that of O. For the same reasons as for O, the abundance of C has also decreased by about 25 %.

The abundance of neon, derived from the ratio Ne/O, also decreased accordingly. The coronal Ne/O ratio, derived from far UV and X-ray lines, has been measured by different authors (Young 2005; Schmelz et al. 2005; Robrade et al. 2008) and has values between 0.15 and 0.20.

Only minor changes are observed between old and new values for heavier elements.

3.1.6 Differences Between Recent Solar Mixtures

Caffau et al. (2011, and references therein) have also recently revisited the solar abundances of a few elements using their own 3D model of the solar photosphere. The results from these authors are slightly larger than those of Asplund et al. (2009): for oxygen, 8.76 compared with 8.69, and for carbon, 8.50, compared with 8.43. The main reasons for these differences are not related to the use of different 3D models. Their somewhat larger O value comes from the forbidden lines and should decrease if the blends were more accurately estimated, the

value from the permitted lines could also somewhat decrease if their solar data as well as the non-LTE results were updated. For carbon, the dispersion in their results is clearly produced by the use of many strong C I lines that are slightly blended leading to a somewhat too large abundance estimate.

In conclusion, Asplund et al. (2009) recommend to use their new solar mixture and discard the old solar mixture of Grevesse and Sauval (1998) that had been used with so much success in the past. Although helium is an important ingredient, it cannot be measured directly in the solar atmosphere and is usually determined helioseismically (e.g. Dappen and Gough 1986; Dziembowski et al. 1991; Kosovichev et al. 1992; Antia and Basu 1994; Richard et al. 1998; Basu and Antia 2004). Assuming a helioseismically determined value of the helium abundance, the new abundance yields a present day solar metallicity of $Z = 0.0134$ with an uncertainty of about 12 %. This uncertainty has been estimated, for the main contributors to Z , by taking into account the combined uncertainties due to the model, to the heterogeneities and to the departures from LTE as recommended by Asplund et al.

Very recently, new 3D models have been built that take solar photospheric magnetic fields into account (Fabbian et al. 2010, 2012; Thaler 2012). These new models might have an influence on the solar abundance results. First estimates of their impact on the O abundance for example, shows a very small increase for the results from the atomic lines and a somewhat larger increase on the abundances derived from the molecular lines. We however need to wait for more severe tests of these new 3D models before being able to really quantify their actual impacts on solar abundances

The problems caused by the lower abundances for solar models and attempts to determine solar abundances using helioseismic data are discussed next.

3.2 Solar Abundances and Helioseismology

Heavy-element abundances affect solar models in a number of ways although the effects are indirect. The main effect is on radiative opacities—higher metallicity implies higher opacities. Opacity in turn affects the position of the base of the outer convection zone and the structure of the radiative zones. Effects of metallicity are also visible in thermodynamic quantities, particularly in the ionisation zones. C, N and O abundances also affect the flux of neutrinos emitted by CNO reactions in the solar core, though the effect is small since CNO reactions account for <2 % of the energy emitted in the Sun. In the case of calibrated SSMs, heavy-element abundances also change the amount of helium required to model the Sun. The changes in the initial helium abundances in SSMs, and the reason, for the change, can be found in Table 6 of Turck-Chièze and Couvidat (2011). Serenelli and Basu (2010) recently determined what the solar initial helium abundance should be by first determining the dependence of the current and initial helium abundance on input parameters and marginalising over them. Assuming the helioseismic $Y_{\text{surf}} = 0.2485 \pm 0.0035$ (Antia and Basu 1994) and a 20 % uncertainty in the diffusion rate, they find $Y_{\text{initial}} = 0.273 \pm 0.006$ independent of the reference model used. Of course, the analysis was limited to SSMs, and non-standard physics could change the results.

The most dramatic manifestation of the change of metallicities is the change in the position of the convection-zone base, which changes the sound-speed difference between solar models and the Sun. In Fig. 3 we show the relative sound-speed and density differences between several solar models of the Sun. The models were constructed with different solar metallicities, but all other inputs were the same. We compare models with the composition of Grevesse and Sauval (1998; henceforth GS98), Asplund et al. (2005; henceforth AGS05),

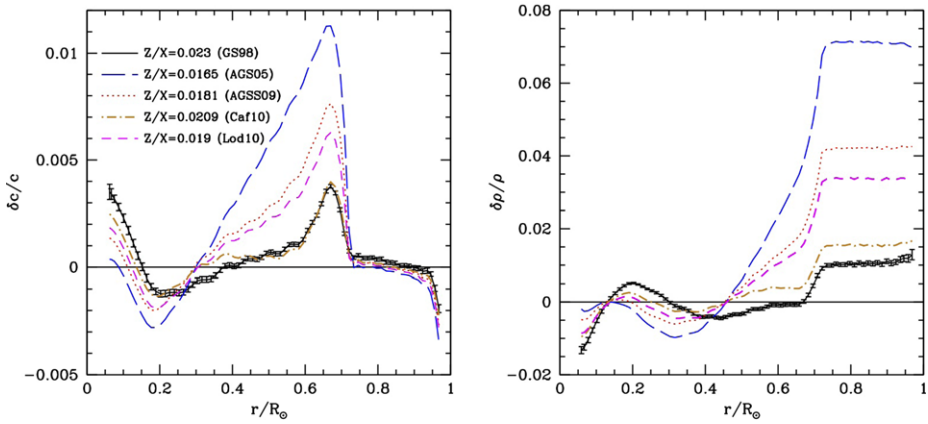


Fig. 3 The sound-speed and density differences between the Sun and standard solar models constructed with different heavy-element abundances. The differences are shown by the *lines* and the *ticks* show 1σ errorbars. For the sake of clarity, errorbars are shown only for one result

Table 1 Properties of models with different heavy-element mixtures

Mixture	Z/X	R_{CZ}	Y_{CZ}	Y_0
Helioseismic	–	0.713 ± 0.001^a	0.2485 ± 0.0034^b	0.273 ± 0.006^c
GS98	0.023	0.7139	0.2456	0.2755
AGS05	0.0165	0.7259	0.2286	0.2586
AGSS09	0.018	0.7205	0.2352	0.2650
CAF10	0.0209	0.7150	0.2415	0.2711
LOD10	0.019	0.7136	0.2412	0.2665

^aBasu and Antia (1997)

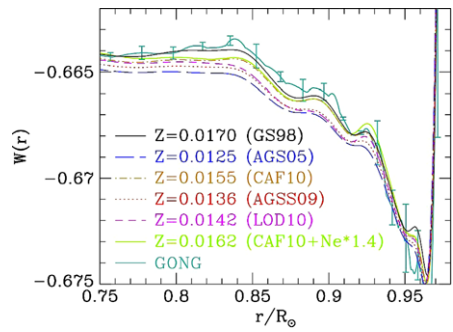
^bBasu and Antia (2004)

^cSerenelli and Basu (2010)

Asplund et al. (2009; AGSS09), Caffau et al. (2010, 2011, CAF10) and the compilation of Loders (2010, Lod10). As can be seen, the AGS05 abundances result in the worst model in terms of sound-speed and density profiles. The newer AGSS09 abundances fare better, but are still less satisfactory compared with the older GS98 abundances or the Caffau et al. (2011) abundances. It is interesting to notice that the Caffau et al. abundances are lower than the GS98 one; however, the sound-speed and density profiles are almost as good because the relative abundances are such that the total opacity is about the same.

The difference in the sound-speed and density is mainly caused by differences in the convection-zone depth. The position of the base of the solar convection zone is known precisely from helioseismology ($0.713 \pm 0.001 R_{\odot}$; Basu and Antia 1997 and references therein), and the lower- Z models do not match that. Also different are the current and initial helium abundances. These are listed in Table 1. As can be seen, the low- Z models also have low helium, lower than what has been determined through helioseismic analyses (see, e.g., Kosovichev et al. 1992; Antia and Basu 1994; Basu and Antia 2004, etc.).

Fig. 4 The dimensionless sound-speed gradient of models constructed with different compositions compared with the solar value as determined using data obtained by GONG, the Global Oscillation Network Group. The model CAF10+Ne·1.4 is a model constructed with CAF10 metallicities where the neon abundance has been increased by a factor of 1.4



There are also, more subtle, signatures in the ionisation zone. In Fig. 4, we show the dimensionless sound-speed gradient of the Sun and the models constructed with different metallicities. This quantity, $W(r)$ defined as

$$W(r) = \frac{r^2}{Gm} \frac{dc^2}{dr}, \tag{1}$$

is sensitive to the changes in the adiabatic index in ionisation zones of various elements. As can be seen, the low- Z models do not agree with the Sun even in the ionisation zones.

As described in Basu and Antia (2008), many attempts have been made to reconcile the new abundances and resulting solar models with the structure of the Sun as determined with helioseismology. Many solutions have been suggested, such as modifying opacities, increasing the rate of gravitational settling that increases the heavy-element abundance at the convection-zone base thereby increasing opacities locally, accretion of low- Z material so that the CZ has lower Z than the interior, etc. None of these steps solve all issues. For instance increasing opacities can bring the CZ base to normal, but that does not change $W(r)$; additionally the opacity changes needed have to be fine-tuned. Increasing the rate of diffusion decreases the convection-zone helium abundance even more. As a result, attempts have been made to determine the solar abundance through helioseismic analyses. This is not simple, since solar oscillation equations do not directly involve abundances, and one has to assume that the inputs to solar models, such as opacity and equation of state, are correct.

Delahaye and Pinsonneault (2006) using helioseismic constraints on the position of the solar convection-zone base and the convection-zone helium abundance first demonstrated that the position of the CZ and the CZ helium abundance of an SSM have different sensitivities to different elements. They used this difference to find that the logarithmic number density of $Fe/H = 7.50 \pm 0.0045 \pm 0.003$ and $O/H = 8.86 \pm 0.041 \pm 0.025$, where the second error term is the uncertainty in the overall abundance scale from errors in the C, N, and Ne. This work assumes that the uncertainties in opacities are given by the difference between OPAL and OP opacities.

To avoid the issue of uncertainties in opacities, Antia and Basu (2006) avoided using constraints sensitive to opacities, and looked to the EOS instead. They assumed that the EOS is correct and calibrated the difference $W(r)$ as a function of a model's metallicity and determined the metallicity for which the $W(r)$ is the same as that of the Sun. They found $Z = 0.0172 \pm 0.002$.

Basu et al. (2007) had shown that the so-called small frequency spacing and frequency ratios between $\ell = 0$ and $\ell = 2$, and $\ell = 1$ and $\ell = 3$ modes are sensitive to the metallicity of the solar core. The frequency ratios are determined by the sound-speed gradient in the core, which in turn is determined by the mean molecular weight and its gradient. Chaplin

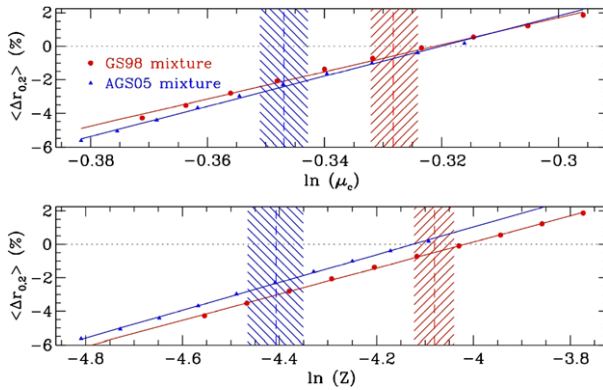


Fig. 5 The relation between the averaged difference of the frequency separation ratios between a solar model and the Sun and the average mean molecular weight in the core of solar models as well as Z for the models. Only results for the (0, 2) separation ratios are shown, results for the (1, 3) ratios are similar. The best-fit straight lines are also shown. The hashed region around these lines represent uncertainties in μ_c and Z . These were obtained from the Monte Carlo simulations of Bahcall et al. (2006). Errors in $\langle \Delta r_{0,2} \rangle$ are of the size of the points

et al. (2007) expanded on this work to use this to determine solar metallicity. They compared the average frequency separation ratios of models with those of the Sun as determined with BiSON data. Chaplin et al. (2007) constructed two sets of test models. The models in each set had different values of Z/X , but one sequence of models was constructed with the relative heavy element abundances of GS98, while the second sequence was made with the relative heavy-element abundances of AGS05. To fix the Z/X of a given model in either sequence, the individual relative heavy element abundances of GS98 (or AGS05) were multiplied by the same constant factor. They found that the mean difference of the separation ratios between the Sun and the models was a linear function of $\ln \mu_c$ and $\ln Z$, where μ_c is the mean molecular weight in the inner 20% (by radius) of the Sun, and Z is the metallicity in the convection zone. This relation can be seen in Fig. 5. This monotonic relationship led the authors to argue that $\ln \mu_c$ and $\ln Z$ for the model that lead to perfect match between the separation ratios of the model and the Sun would be a good estimate of $\ln \mu_c$ and $\ln Z$ of the Sun. They found that the relative abundances of GS98 yielded a solar Z of 0.0178 and the AGS mixture a solar Z of 0.0161.

Thus most helioseismic analyses thus far have yielded high solar metallicities, bringing them into conflict with some of the new spectroscopic measurements that have been discussed earlier. It should be noted though that some analyses yield a low metallicity (see e.g., Vorontsov et al. 2013).

As mentioned earlier, changing the most obvious inputs does not bring models with low abundances back in concordance with the Sun. There are ongoing efforts that assume that the new abundances are correct and look to neglected physics, such as those discussed in Sects. 5 and 6 to bring solar models back in agreement with the Sun.

4 The Solar Equation of State

The ability of helioseismology to probe the solar interior in such detail has allowed us not just to determine solar structure and dynamics, but also to use the Sun as a laboratory to test

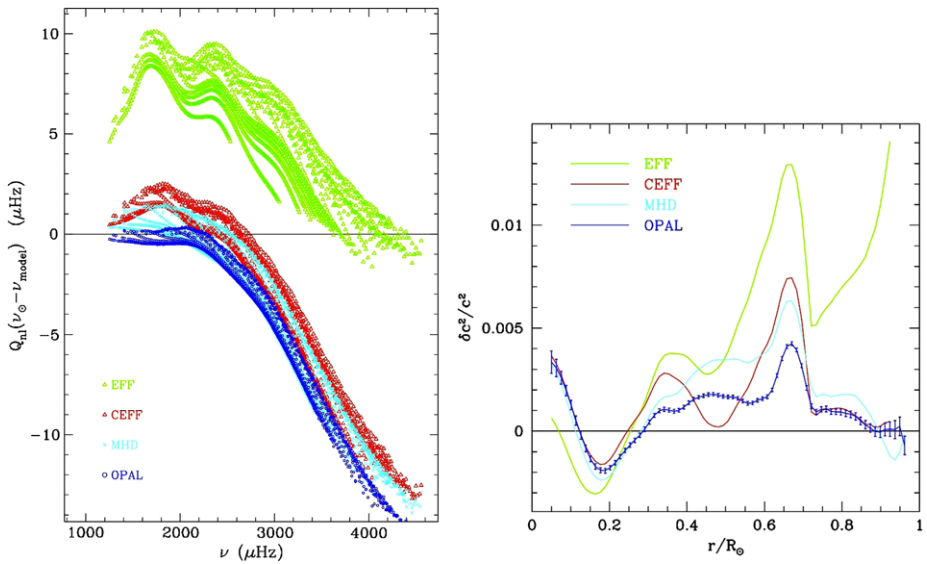


Fig. 6 *Left*: The scaled frequency differences between the Sun and SSMs constructed with different EOSs. The factor Q_{nl} corrects for the fact that frequencies of modes with low inertia change more for the same perturbation than frequencies of modes with high inertia. *Right*: The relative sound speed differences between the Sun and the models. Note that the models were constructed with the Grevesse and Noels (1993) abundances

different inputs that are used to construct solar models. One of these inputs is the equation of state (EOS). The EOS provides a relation between pressure, temperature, composition and abundances. It is a description of the fundamental properties of matter. The equation of state determines the structure of the ionization zones and the convection zone and as a result, determines the structure of the model.

Equations of state that are used as inputs in stellar models are results of extremely complicated theoretical calculations. Thus there is no certainty that they are correct, and hence they need to be tested. An indirect way to examine whether an EOS is correct is to construct an SSM with the EOS and examine its frequencies and sound-speed profile. An example of this is shown in Fig. 6. In these figures we show the frequency difference between the Sun and the models constructed with different EOSs but otherwise identical inputs. These are the Eggleton, Faulker and Flanery (EFF; Eggleton et al. 1973) EOS, a relatively simple EOS that is still used by many stellar modellers, the Coulomb Corrected EFF (CEFF; Christensen-Dalsgaard and Daeppen 1992) EOS which is basically the EFF EOS but with Debye-Hückel Coulomb corrections that rectifies its absence in EFF EOS, the so-called MHD equation of state (Dappen et al. 1987; Hummer and Mihalas 1988; Mihalas et al. 1988) and the OPAL equation of state (Rogers et al. 1996; Rogers and Nayfonov 2002). The last two are results of complex theoretical calculations.

As is clear from Fig. 6 (left) we can see that the model with EFF EOS fares very badly. The other EOSs are better, the differences between them appear smaller, and the frequency differences alone are not enough to indicate whether the EOS are good since the frequency differences are dominated by differences in the near surface layers. Hence in Fig. 6 (right) we show the sound-speed differences between the models and the Sun. Note that one can see that OPAL models do better than MHD and CEFF. CEFF looks marginally better. The

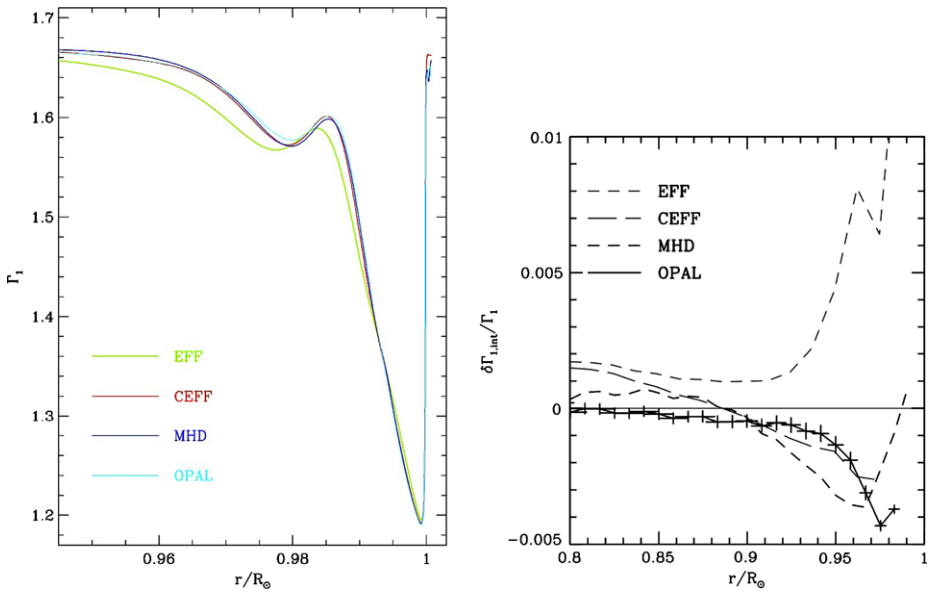


Fig. 7 *Left:* The Γ_1 profiles of models constructed with different EOSs. *Right:* The intrinsic Γ_1 differences between the Sun and models constructed with different EOSs

CEFF EOS is however not fully thermodynamically consistent (see Christensen-Dalsgaard and Daeppen 1992).

The sound-speed profile is an indirect way to test the EOS. A somewhat more direct way is to examine the profile of the adiabatic index Γ_1 . The adiabatic index was used by Elliott and Kosovichev (1998) to show that the then available versions of OPAL and MHD were deficient under conditions present in the solar core. It was found that Γ_1 for the solar core was less than $5/3$ while that of the models was $5/3$. The decrease in Γ_1 in the solar core was attributed to the relativistic tail of the velocity distribution of electrons. The deficiency in the input EOSs has since been rectified (Turck-Chièze et al. 2001; Gong et al. 2001; Rogers and Nayfonov 2002).

The ionisation zones are good regions to study the equation of state since the process of ionisation changes Γ_1 . This is particularly true for the He II ionisation zone which leaves a marked dip in Γ_1 (see Fig. 7[left]). The He I ionisation zone is less useful since the H I ionisation zone merges with it. However, Γ_1 also depends on the helium abundance of the models (which we cannot specify), and the ionisation zone also depends on other structural quantities. Basu and Christensen-Dalsgaard (1997) proposed a way of studying the part of Γ_1 (what they called the “intrinsic” Γ_1) that is independent of structure and helium abundance. The intrinsic Γ_1 differences between the Sun and several EOS are shown in Fig. 7(right). Note that we find again that EFF is very deficient, that OPAL does better than MHD in the deeper layers, however, closer to the surface MHD does better. Basu et al. (1999) confirmed that MHD indeed does better than OPAL in the outermost layers and could attribute that to the treatment of H II.

As we can see above, none of the input equations of state describe the EOS of the solar material perfectly and more work needs to be done in this regard. One of the biggest drawbacks of both MHD and OPAL EOSs is that they are both constructed with a fixed relative-abundance of heavy metals. This makes testing new abundances difficult.

CEFF allows the flexibility to changing relative-abundance, however, it is not a completely thermodynamically consistent EOS and this shows up as discrepancies in the deeper layers of the Sun. Fortunately for abundance tests, the outer layers of the Sun are described well by the CEFF EOS. There are some analytic EOS that have been developed in recent years and these are not-only thermodynamically consistent, but also allow the Z mixture to be changed. These include the SIREFF EOS (Guzik and Swenson 1997; Guzik et al. 2005). The use of this EOS shows that changing the relative abundance in the EOS does not change the sound-speed profile of the models enough to alleviate the problem with the low abundances (Guzik and Mussack 2010).

5 Towards a Better Description of the Solar Radiative Zone

Helioseismology has given us new, detailed information about the solar radiative zone that exposes the limits of SSMs. In this section we discuss some of the differences between the Sun and SSMs which could be connected to the limitations of these standard models and the equations used to construct them. In particular we focus on questions related to energy transport. The next section is dedicated to dynamical processes.

5.1 The Energy Balance, Neutrino Fluxes and the Central Composition

It is instructive to compare the central conditions obtained in SSMs with those of seismic models that reproduce the solar sound speed and density profiles. Seismic models suggests that the central temperature of the Sun is slightly greater than the central temperature of current SSMs and that the Sun also has a slightly greater central density (Turck-Chièze et al. 2011). The 1.5 % difference in temperature has important consequences for the prediction of the Boron neutrino flux which has an extremely high temperature-dependence (a factor of about 20). This flux has been measured by the SNO detector and is directly comparable to predictions unlike other neutrino fluxes that require neutrino flavour-transformations to be taken into account. The prediction of the seismic model is in perfect agreement with this detection: 5.31 ± 0.6 for a detected value of $5.045 \pm 0.18 \times 10^6 \text{ cm}^{-2} \text{ s}^{-1}$ but the SSM prediction is a bit too low 4.5 ± 0.5 (Turck-Chièze and Couvidat 2011). This difference could be interpreted as an energy-generation related problem in SSMs that neglect any motion in the whole radiative zone; this energy difference is easy to quantify. Since p - p reactions dominate solar nuclear burning, one can estimate a maximal difference of 5–6 % between the energy production and its release at the surface between the Sun and SSMs. SSMs assume that the produced energy is transported only by photons. Assuming this is correct, the discrepancy between the sound speed and density profiles between the radiative zones of the Sun and models can be explained as being partly due to a redistribution of the produced energy through other energetic phenomena that are not included in SSMs. Possible candidates include magnetic energy, kinetic energy, meridional circulation energy in the radiative zone, gravity wave energy, and dark matter energy that can be additional channels for the transport of energy.

Making progress on these points is difficult, but this may be possible in the near future thanks to some complementary observables: a better detection of gravity modes (see the description of the instrument called GOLD in the chapter dedicated to future projects) for a much improved determination of the dynamics of the core and the use of the neutrino spectroscopy to determine the electron density totally independently (Lopes and Turck-Chièze 2013). The transport of energy by photons and microscopic diffusion in the radiative zone will be checked by the ^{13}N and ^{15}O neutrino fluxes; the accurate measurement of the pep neutrino flux will constrain the energy produced by the p - p chain.

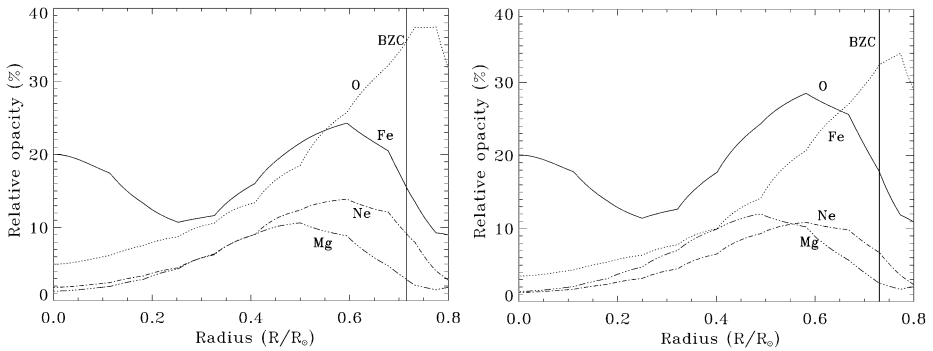


Fig. 8 Main contributions of heavy elements to the total opacity for: *Left*: the GS98 composition, and *Right*: the AGS05 composition. ‘BCZ’ marks the base of the convection zone. From Turck-Chièze et al. (2009)

5.2 Energy Balance and Dark Matter

Twenty years ago, the idea that weakly interactive massive particles (WIMPs) could slightly lower the solar central temperature had been explored to help solve the solar neutrino problem. Today these particles remain very good candidates for dark matter, but the problem is reversed. Since the core of the Sun shows no evidence of cooling, the absence of WIMPs’ signatures put some limits on their mass: masses ≤ 12 GeV are excluded for currently accepted interaction cross sections (Turck-Chièze et al. 2012; Turck-Chièze and Lopes 2012). This result is also supported by other studies and the mass of these particles is mainly assumed around 100 GeV, a value that is not easy to detect.

Other particles, like axions and sterile neutrinos, are also considered to be potential candidates for dark matter. If these particles are present in the Sun, they will act very differently on the solar interior. They will indeed transport energy in the whole radiative zone but their very low mass means that they will not migrate to the most central regions; however, they could modify the gravitational field in the radiative zone. This justifies a dedicated study to determine their specific density and interactions.

5.3 The Transport of Energy by Photons

The equations governing SSMs only consider the production of energy by nuclear reaction and the instantaneous energy loss by neutrinos. The energy is transported by photons in the radiative zone of the Sun. This transport is calculated using Rosseland mean opacity tables which result from calculations using the local mixture of elements. Current SSMs use the work derived by Iglesias and Rogers (1996) or those of the OP consortium (Badnell et al. 2005). These calculations represent the best estimates of such complex calculations. The recent revisions of solar metallicity have deteriorated the earlier good agreement between the sound-speed and density profiles of the Sun, mainly through modification of opacity because of changes in O and Fe (Christensen-Dalsgaard et al. 2009; Turck-Chièze et al. 2009).

Figure 8 shows how the changes in relative abundances modifies the role of the main contributors to the total opacity. The contribution of oxygen was at the level of iron for the GS98 composition in a large part of the radiative zone; when the oxygen abundance is reduced, the iron contribution becomes dominant. The newer AGS09 composition gives rise to an intermediate situation. The shape of the oxygen contribution has the opposite shape

of the change in the sound-speed differences between the Sun and models with GS98 and AGS05 compositions (see Fig. 3), this is not completely surprising, since ultimately the change in the O abundance is the main reason for the difference in sound speed between the two models.

The opacity calculations have never been validated through measurements made for solar conditions. New possibilities for making such measurement exist today using the Z machine (Bailey et al. 2007) and large laser facilities (Turck-Chièze et al. 2009). In parallel, new detailed calculations of opacity are being performed to better describe the transport of energy and for the microscopic diffusion of elements that can change local opacities (Blancard et al. 2012; Turck-Chièze and the OPAL consortium 2013). Another effort is underway to improve the grids of calculated opacities for conditions near the base of the convective zone, as well as improve interpolation between the grids.

6 A Dynamical View of the Inner Sun

SSMs and most stellar models ignore dynamical processes and hence avoid issues such as the transport of angular momentum from one part of the star to another. However, the Sun and solar-type stars are dynamical and magnetic objects, and hence, rotation and magnetic fields could modify their evolution as well as their interaction with their external environment. We know, for example, that differential rotation induces “non-standard” mixing processes, which modify their lifetime, their late stages of evolution and their nucleosynthetic properties (e.g., Maeder 2009). Since we now have strong constraints on the Sun’s internal rotation (e.g. Schou et al. 1998; García et al. 2007, 2011a; Turck-Chièze and Lopes 2012) and on more evolved low-mass stars (e.g. Beck et al. 2012; Deheuvels et al. 2012; Mosser et al. 2012), it is time to construct solar and stellar models that account for magneto-hydrodynamic effects on both dynamical and secular time-scales. In this section, we describe recent progress that has been made in the detection and modelling of secular exchanges of angular momentum in the Sun and low-mass stars interiors focusing on mechanisms that act in the radiative core. Readers are referred to Brun (2011) for processes in the convective region.

6.1 The Role of the Turbulence

While dynamical processes are generally not included in SSMs, one process, namely convection, has to be included, and this is usually done using the “mixing length theory,” or MLT (Böhm-Vitense 1958). MLT assumes that the full range of turbulent eddies can be parametrized with a single parameter, the mixing length parameter α . In the case of the Sun, this parameter can be calibrated by requiring the Sun to have its observed radius and luminosity at its current age. The solar calibrated value of α is normally used for all other stars, although there is increasing evidence that the solar α should not be used in other stars (see Bonaca et al. 2012, and references therein). In addition to the large-scale convective motions, turbulence is present in two regions: the base of the convection zone and the subsurface layers. The high-precision of the available seismic data justifies paying more attention to these regions.

6.1.1 Turbulence Below the Convective Envelope

There are two possible sources of turbulence in this region:

- Dynamical shear-induced turbulence caused by the horizontal shear imposed at the top of the stably stratified radiative zone by turbulent flows in the surrounding convective envelope (Zahn 1992; Spiegel and Zahn 1992), this case is discussed in Sect. 6.2.
- Turbulence due to the penetration of convective flows into the radiation zone because of their inertia, commonly referred to as convective overshoot (e.g. Zahn 1991; Brun et al. 2011).

An interesting point is that both sources of turbulence may lead to efficient mixing at the base of the convective envelope that reduces the differences between the sound-speed profile of a solar model and the Sun (e.g. Richard et al. 1996; Brun et al. 1999; Zhang et al. 2012).

6.1.2 Turbulence in the Subsurface Layers

Treating this region correctly is particularly important in improving predictions of acoustic-mode frequencies and also in understanding the 2-year modulation (Fletcher et al. 2010) and 11-year cycles (Elsworth et al. 1990; Libbrecht and Woodard 1990, etc.) seen in solar acoustic mode frequencies. SSMs do not include the effects of turbulence on solar structure, and this leads to the large frequency-dependent discrepancy between the solar frequencies and those of the models (see Fig. 6[Left]). Realistic 3D simulations of the convection zone show that turbulent pressure plays a role in an extended region just below and just above the surface (e.g., Nordlund et al. 2009) with a consequent modification of density and thermal structure. This leads to a direct effect on the predicted radius and in the predicted frequencies. This significantly reduces the frequency differences between models and the Sun (Rosenthal et al. 1999; Li et al. 2002, etc.). Additionally one can introduce magnetic field in the 3D code to study how the solar radius evolves with activity. First results, using the strength of the toroidal field as determined by Baldner et al. (2009) from seismic observations, can be found in Piau et al. (2014).

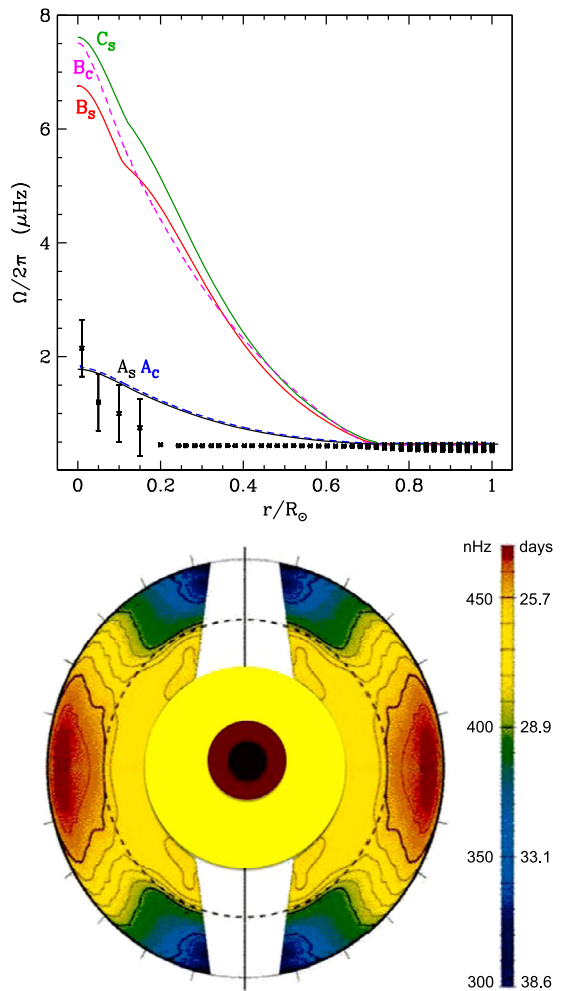
6.2 The Solar Rotation Profile

Early helioseismic results had shown that the surface latitudinal differential rotation (25 days around the equator up to 32 days at 75 degrees) is maintained throughout the convective zone but disappears in the turbulent layers called “tachocline” located at the transition between radiative and convective zone. A more or less rigid rotation in the radiative zone is observed down to the limit of the core (Eff-Darwich and Korzennik 2012).

It is well known that acoustic modes contain very little information about the rotation of the solar core. This is because they have their largest amplitudes close to the surface and very few modes penetrate to the core. By contrast, gravity (or *g*) modes are the natural way to probe the solar core but due to their evanescence in the outer convective zone, they are particularly difficult to detect. Their predicted amplitude is at the level of mm/s at the surface (Belkacem 2011).

The unique performance of the GOLF instrument at low frequencies (see Turck-Chièze and Lopes 2012) and its exceptionally long stretch of observations has made GOLF observations the prime dataset to look for *g*-modes. Some candidates have been found in the mixed mode range after integration over more than 4 years of observations (Gabriel et al. 2002; Turck-Chièze et al. 2004b). The most probable detections correspond to mixed modes of $\ell = 2$, $n = -3$ that are believed to be the most easily excited in that range of frequencies (Cox and Guzik 2004). The search was conducted again with more than 10 years of GOLF data (García et al. 2008). Another search was done after adding the mode power spectra in the asymptotic range where the modes are nearly equidistant in period (García et al. 2007)

Fig. 9 *Top*: Comparison of the solar rotation profile as obtained with a combination of MDI and GOLF data with different predictions made by including transport of momentum by rotation. The data points with errorbars are results obtained using a combination of GOLF and MDI data. The label S stands for the STAREVOL code and C for CESAM code. ‘A’ corresponds to a very slow initial rotation, ‘B’ and ‘C’ correspond respectively to initial rotation rates of 20 km/s and 50 km/s; see Turck-Chièze et al. (2010a) for details. At the scale of the axes, the latitudinal differential rotation of the convective zone is not visible clearly. *Bottom*: 2D schematic of the solar internal rotation profile obtained with SoHO data

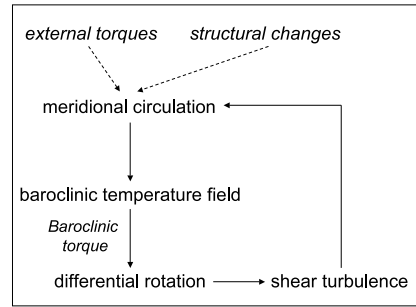


and then looking directly to the region located between 90 to 200 μHz (García et al. 2011b). García et al. (2011b) claimed significant (>99.99 % confidence level) excess power that they attributed to dipole modes ($\ell = 1$). The patterns were compatible with larger splittings in the solar core region than those obtained from acoustic modes. The gravity mode splittings, combined with acoustic mode splittings obtained from GOLF and MDI observations, lead to a first insight on the rotation profile in the whole Sun. The rotation rate in the core appears a factor between 5 and 8, depending on the detailed shape in the core, greater than the rest of the radiative zone (see Fig. 9 top). Such results are also seen with asteroseismology for other stars as mentioned earlier and motivate the construction more complete models of the Sun that include the transport of momentum by rotational mechanisms as suggested by Zahn (1992) and Mathis and Zahn (2004).

6.3 The Transport of Momentum by Rotation During the Sun’s Lifetime

One first needs to understand differential rotation and the associated large-scale meridional circulation, and shear-induced turbulence (e.g. Zahn 1992; Maeder and Zahn 1998; Mathis

Fig. 10 The transport loop in stellar radiation zones when differential rotation, the associated large-scale meridional circulation and shear-induced turbulence are taken into account. From Decressin et al. (2009)



and Zahn 2004). Rieutord (2006) and Decressin et al. (2009) give a global view of the coupling of the various processes involved. First, viscous turbulent transport, stellar winds and structural adjustments induce meridional currents. These currents advect heat and that in turn leads to a latitudinal gradient of temperature. Because of the associated baroclinic torque, a new differential rotation profile is built which can be understood looking at the so-called thermal-wind equation, and this closes the transport loop (see Fig. 10).

The surface of the Sun rotates today slowly at about 2 km/s. However, it is generally believed that young stars rotate fast, slowing down after several millions of years. This slow-down is believed to be a result of magnetic braking and angular momentum is redistributed through advection by the meridional circulation and diffusion by the shear-induced turbulence (Zahn 1992; Maeder and Zahn 1998; Mathis and Zahn 2004). The first comparison of the solar rotation profile with detailed models that included rotation showed that the observed rotation in the core is lower than thought theoretically (see Fig. 9). The present rotation profile of the whole Sun also remains difficult to explain. Another result is that the introduction of this dynamical process does not reduce the difference between the observed sound speed profile and that of such models (Turck-Chièze et al. 2010a).

The main conclusions of Turck-Chièze et al. (2010a) can be summarized as follows:

- In the different cases that have been studied, and that vary in their initial rotation rate (50 km/s, 20 km/s and extremely small), the meridional circulation of the radiative zone becomes extremely slow in comparison with the observed meridional circulation in the convective zone. Consequently, the tachocline appears naturally as a very turbulent region, with horizontal motions. Thus there exist two very different dynamical regimes in addition to the two different regimes of transfer of energy. The calculated radiative-zone meridional velocities are smaller than those used in existing 3D simulations; these simulations of course cannot yet handle the secular evolution of the transport of angular momentum over Gyrs.
- In all cases, the transport of angular momentum was efficient mainly during the contraction phase (where core rotation increases rapidly) and during the pre-main-sequence. The transport of momentum by rotation is largely reduced during the main sequence.
- When the initial rotation rate is high (20–50 km/s), the current core rotation is too high compared with the observed value, so one possibility is that the Sun was a rather slow rotator (5–10 km/s) and the other is that the rotation rate has been reduced by some other process. Moreover, none of the calculations lead to the observed rigid rotation out of the solar core. These two facts suggest that some additional transport of momentum had been effective in the past and may be effective even today.

Thus the present solar core rotation profile appears to be a relic of the first million years of the Sun's life and its knowledge requires a better description of the young Sun, in particular, of the phases I and II of evolution as described by Lada (1987), Andre et al. (2000).

Differential rotation and associated meridional currents and shear-induced turbulence, if applied to the Sun and low-mass stars, are unable to reproduce the angular-velocity profile of the radiative core of the present Sun (Pinsonneault et al. 1989; Turck-Chièze et al. 2010b). They cannot reproduce light-element mixing in solar-type stars on the main sequence (e.g. Talon and Charbonnel 2005) either. Nor can they reproduce the rotation profiles of the central radiation zone of low-mass subgiant and red giant stars (Eggenberger et al. 2012; Ceillier et al. 2012; Marques et al. 2013). Thus other processes, such as magnetic fields (e.g. Rudiger and Kitchatinov 1997; Gough and McIntyre 1998; Garaud and Garaud 2008; Wood et al. 2011) or internal waves excited by penetrative convection (e.g. Schatzman 1993a; Zahn et al. 1997) must be studied.

6.4 The Transport of Momentum by Magnetic Fields

Another possible mechanism of angular momentum transport is the magnetic field that could have been built when the Sun was young. This was an epoch when the Sun was certainly much more active than it is today; the Sun at that epoch was fully convective as well. During this phase, a dynamo effect could have amplified an initial field in the proto-stellar cloud. At that time, when the star is a few Myrs old, mass loss could become largely greater than accretion leading to a loss of angular momentum. Spectropolarimetry today shows complex magnetic field configuration for such stars (Donati and Landstreet 2009). Eggenberger et al. (2005) have also suggested that a fossil field in the Sun can lead to a strictly uniform core rotation that matches with helioseismology in contrast to angular momentum extraction by gravity waves. Of course, these two processes can act simultaneously in the present Sun (Mathis 2013).

A reasonable model of the young Sun that contains all the phenomena observed in the other young stars is not yet available. Such a model must contain not only an appropriate, realistic, magnetic field configuration and its effect on the solar rotation, but also mass loss. Such magnetic fields, if they subsist in time, will be subject to Ohmic diffusion and to advection by the shear of differential rotation and meridional currents, and will transport angular momentum to damp differential rotation in the whole radiative zone. Some preliminary studies can be found in Duez et al. (2010b), Turck-Chièze et al. (2011). Indeed this is the most accepted hypothesis for the origin of magnetic fields in the cores of solar-type stars (Mestel 1965). One first needs to understand the field geometry in the radiation zone since it affects angular momentum transport. This problem is related to magneto-hydrodynamic relaxation processes, wherein an initial turbulent magnetic field is converted into a large-scale configuration thanks to a selective decay of the ideal magneto-hydrodynamic invariants. The case of the high- β stellar radiation zone plasma, where gas pressure dominates, has been studied both theoretically (Duez and Mathis 2010) and numerically (Braithwaite and Spruit 2004; Braithwaite and Nordlund 2006; Braithwaite 2008). Roughly axisymmetric dipolar twisted configurations are obtained if the initial magnetic energy is confined near the centre (Braithwaite and Nordlund 2006; Duez and Mathis 2010), while one gets non-axisymmetric fields in the case where the energy is distributed in the whole radiation zone (Braithwaite 2008). The field is then organised on large scales, mixed (poloidal and toroidal), non force-free configurations, which are in-

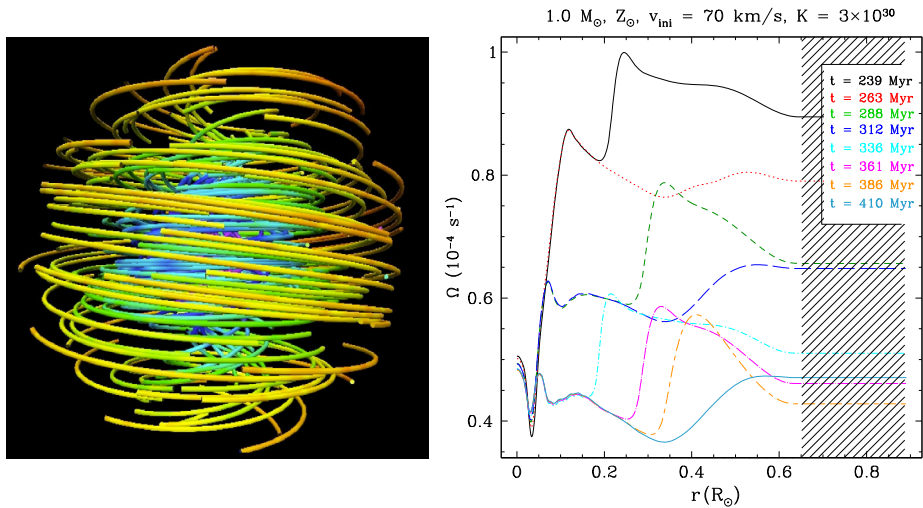


Fig. 11 *Left:* 3-D topology of an axisymmetric relaxed fossil magnetic field (from Duez et al. 2010a, 2010b). In the case of such configuration, the angular velocity will be frozen along the lines of the poloidal (i.e. meridional) component of the field. *Right:* Net extraction of angular momentum by internal waves in a solar-type star. The braking applied by the wind induces the extraction of angular momentum along a front created because of the propagation of retrograde waves deep in the core. *Hatched areas* indicate the convective envelope. from Alvan et al. (2013)

tially stable as has been demonstrated by Braithwaite (2009) and Duez et al. (2010a) (see Fig. 4 of Duez et al. 2010a).

Once the initial relaxed magnetic configuration has been established (see left panel of Fig. 11), it interacts with differential rotation. In the case of axisymmetric configurations, the rotation becomes uniform on poloidal (i.e. meridional) magnetic surfaces; this is the so-called Ferraro-state (e.g. Brun and Zahn 2006; Spada et al. 2010; Strugarek et al. 2011a). In the case of a non-axisymmetric field, the rotation will become uniform if the field is strong (e.g. the oblique rotators case; see Moss 1992) while the case of a weak field is being explored (see Spruit 1999; Strugarek et al. 2011b). This picture could be modified by magnetic instabilities if during the first phase of evolution the residual differential rotation on each magnetic surface is able to generate a strong toroidal component of the field that becomes unstable (e.g. Tayler 1973), and if this instability is able to trigger a dynamo action through an α -effect. This question is strongly debated (Spruit 2002; Zahn et al. 2007; Rüdiger et al. 2012).

Finally, let us examine the interaction of fossil fields with meridional currents. Meridional flows in radiation zones are driven by internal viscous and magnetic stresses, by external torques such as those due to stellar winds, and by structural adjustments during stellar evolution. In the case where all these sources vanish, the meridional circulation dies after an Eddington-Sweet time and the star settles in a baroclinic state described by the magnetic thermal wind equation. When applied to magnetised radiation zones of a star without structural adjustments and external torques, the meridional circulation will thus be mainly driven by the residual Lorentz torque until the star reaches a torque-free state and the advection of angular momentum by meridional circulation balances the residual magnetic torque (see Mestel et al. 1988; Mathis and Zahn 2005).

6.5 Internal Waves

The last transport mechanism that we consider here is the action of internal waves propagating in the stably stratified radiative cores of the Sun and solar-type stars. These are excited by turbulent convective flows at the radiation/convection border (e.g. Garcia Lopez and Spruit 1991; Dintrans et al. 2005; Rogers and Glatzmaier 2005; Belkacem et al. 2009). These waves transport angular momentum, which is deposited where waves are damped because of thermal diffusion (e.g. Zahn et al. 1997) or where they meet their co-rotation layers (Goldreich and Nicholson 1989; Alvan and Mathis 2011). In case of prograde waves, the momentum flux is of the same sign as that of energy flux leading to a deposition of angular momentum. For retrograde waves, the momentum and energy fluxes are of opposite signs leading to an extraction of angular momentum. Then, if a negative gradient of differential rotation is initially present, a net extraction of angular momentum is obtained because of the Doppler effect that leads to a stronger damping of prograde waves which are thus damped closer to the excitation region. Then, different angular momentum extraction fronts propagate from the interior to the exterior during the evolution (see Fig. 11 [right]). This extraction, combined with the strong horizontal shear-induced turbulence due to the stable stratification, is therefore a possible explanation of the observed quasi-uniform rotation rate in the inner $0.2 R_{\odot}$ of the solar radiative zone, as well as an explanation of mixing in low-mass stars (Charbonnel and Talon 2005; Talon and Charbonnel 2005). Additionally, when the action of internal waves is efficient, meridional circulation is strongly affected and becomes highly multi-cellular because of Reynolds stresses.

Progress still needs to be made in the description of wave-excitation by turbulent convection (Brun et al. 2011; Alvan et al. 2012; Lecoanet and Quataert 2013) and on the impact of rotation and magnetic fields on their propagation, dissipation and on the induced transport of angular momentum. Indeed, the young Sun was rotating faster than the current Sun with an internal differential rotation caused by contraction and braking. The tachocline is believed to be the place of the large-scale toroidal magnetic field storage in the Sun (Browning et al. 2006). This is why the changes in the structure of the waves and their dissipation by differential rotation and by magnetic fields have been studied (Mathis et al. 2008; Mathis 2009; Mathis and de Brye 2011, 2012). The waves become Magneto-Gravito-Inertial waves because of the three restoring forces: i.e. the buoyancy force, the Coriolis acceleration, and the Lorentz force. Then, depending on the ratio between excited frequencies (σ_c), the inertial frequency (2Ω , where Ω is the angular velocity) and the Alfvén frequency (ω_A), the propagation of these waves can be strongly modified. First, in the case of an axisymmetric toroidal field (e.g. Schatzman 1993b; Kim and MacGregor 2003; Rogers and MacGregor 2011; Mathis and de Brye 2011), waves become vertically trapped as soon as $1 - m^2\omega_A^2/\sigma_c^2 < 0$ (where m is the azimuthal order). Next, for such a field geometry, low-frequency waves (for example sub-inertial ones for which $\sigma_c < 2\Omega$) become trapped in an equatorial belt below a given critical latitude with a stronger trapping for prograde waves when the magnetic tension force is taken into account. This modifies the transmission of energy from turbulent convection to waves which is reduced in the case of trapped waves. Moreover, the thermal diffusion of waves is enhanced as soon as the rotation and the field amplitude is increased leading to a damping closer to the excitation region. The efficiency of the induced transport of angular momentum is thus a function of the rotation and of the field amplitude. It decreases as soon as vertical and horizontal trapping of wave modify wave-dynamics, with a net bias in favor of retrograde waves (see details given in Mathis and de Brye 2012).

6.6 The Coupling of the Sun and Other Solar-Type Stars to Their Surroundings

As has been emphasised in previous sections, torques applied on a star's outer envelope modify internal transport processes: for instance they can drive the large-scale meridional circulation (e.g. Zahn 1992). Therefore, one must get a coherent physical model of the interaction of the Sun and solar-type stars with their environment when their rotational evolution is studied (Bouvier 2008). First, stellar winds must be carefully examined as a function of a star's rotation rate and of its magnetic field topology and amplitude (e.g. Kawaler 1988; Pinto et al. 2011; Matt et al. 2012). Furthermore, if the star under scrutiny hosts a planetary system, the coupling with the proto-planetary disk (Matt and Pudritz 2005; Zanni and Ferreira 2013) and tidal interactions should be taken into account. For the latter, the equilibrium tide applied to the hydrostatic adjustment of the star to the tidal excitation, leads to a net torque applied on the outer convective envelope of solar-type stars (Zahn 1966; Remus et al. 2012) and this modifies their rotational evolution (Zahn and Bouchet 1989). Moreover, internal waves are also excited by the tidal potential at the radiation/convection boundary and are able to transport angular momentum in the same way that those excited by the turbulent penetrative convection: this is the so-called dynamical tide (see e.g. Zahn 1975; Ogilvie and Lin 2007). Therefore, we find that one needs a detailed picture of the secular exchanges of angular momentum to get a precise and exact picture of the structure and evolution of the Sun and solar-type stars. Constraints from helio- and asteroseismology will probably be our best guide.

7 Concluding Thoughts

The solar model is a work in progress. In this article we have tried to give a flavour of some of the uncertainties in the model ingredients, such as abundances and the equation of state, and discuss one of the most neglected physical properties, namely angular momentum transport.

Abundances and equation of state are important ingredients for all solar models. We have described the painstaking analysis needed to measure solar abundances from solar spectra. We have also discussed the current discrepancy between abundance estimates from helioseismic analyses and spectroscopic analyses. We have also shown how equations of state can be tested and the state of the currently used equations of state.

An examination of what seismic data reveals about the radiative zone and comparing the results models reveals the limitations of standard solar models. The equations of standard solar models need to be supplemented with equations that describe dynamical evolutions and angular momentum transport. We have described some of the ways angular momentum may be transported in the Sun. Seismic data also point the way to investigations into other interesting processes that may play a role in transporting energy from the solar core, including gravity mode propagation, neutrinos, plasma processes and perhaps even dark matter. We expect the next generation of observations and experiments to provide better constraints on these ingredients.

References

- M.C. Abrams, A. Goldman, M.R. Gunson, C.P. Rinsland, R. Zander, *Appl. Opt.* **35**, 2747–2751 (1996)
- C.W. Allen, *Astrophysical Quantities* (1973)
- L. Alvan, S. Mathis, Critical layers for internal waves in stellar radiation zones, in *SF2A-2011: Proceedings of the Annual Meeting of the French Society of Astronomy and Astrophysics*, ed. by G. Alecian, K. Belkacem, R. Samadi, D. Valls-Gabaud (2011), pp. 443–447

- L. Alvan, A.S. Brun, S. Mathis, 3D simulations of internal gravity waves in stellar interiors, in *SF2A-2012: Proceedings of the Annual Meeting of the French Society of Astronomy and Astrophysics*, ed. by S. Boissier, P. de Laverny, N. Nardetto, R. Samadi, D. Valls-Gabaud, H. Wozniak (2012), pp. 289–293
- L. Alvan, S. Mathis, T. Decressin, *Astron. Astrophys.* **553**, A86 (2013). doi:[10.1051/0004-6361/201321210](https://doi.org/10.1051/0004-6361/201321210)
- E. Anders, N. Grevesse, *Geochim. Cosmochim. Acta* **53**, 197–214 (1989)
- P. Andre, D. Ward-Thompson, M. Barsony, *Protostars and Planets IV*, p. 59 (2000)
- H.M. Antia, *Astron. Astrophys.* **307**, 609–623 (1996)
- H.M. Antia, S. Basu, *Astrophys. J.* **426**, 801–811 (1994)
- H.M. Antia, S. Basu, *Astrophys. J.* **644**, 1292–1298 (2006)
- M. Asplund, N. Grevesse, A.J. Sauval, in *Cosmic Abundances as Records of Stellar Evolution and Nucleosynthesis*, ed. by T.G. Barnes III, F.N. Bash. *Astronomical Society of the Pacific Conference Series*, vol. 336 (2005), p. 25
- M. Asplund, N. Grevesse, A.J. Sauval, P. Scott, *Annu. Rev. Astron. Astrophys.* **47**, 481–522 (2009)
- N.R. Badnell, M.A. Bautista, K. Butler, F. Delahaye, C. Mendoza, P. Palmeri, C.J. Zeippen, M.J. Seaton, *Mon. Not. R. Astron. Soc.* **360**, 458–464 (2005)
- J.N. Bahcall, M.H. Pinsonneault, G.J. Wasserburg, *Rev. Mod. Phys.* **67**, 781–808 (1995). doi:[10.1103/RevModPhys.67.781](https://doi.org/10.1103/RevModPhys.67.781)
- J.N. Bahcall, M.H. Pinsonneault, S. Basu, *Astrophys. J.* **555**, 990–1012 (2001)
- J.N. Bahcall, A.M. Serenelli, S. Basu, *Astrophys. J. Lett.* **621**, 85–88 (2005)
- J.N. Bahcall, A.M. Serenelli, Sarbani Basu, *Astrophys. J. Suppl. Ser.* **165**, 400 (2006). doi:[10.1086/504043](https://doi.org/10.1086/504043)
- J.E. Bailey, G.A. Rochau, C.A. Iglesias, J. Abdallah Jr., J.J. Macfarlane, I. Golovkin, P. Wang, R.C. Mancini, P.W. Lake, T.C. Moore, M. Bump, O. Garcia, S. Mazevet, *Phys. Rev. Lett.* **99**(26), 265002 (2007)
- C.S. Baldner, H.M. Antia, S. Basu, T.P. Larson, *Astrophys. J.* **705**, 1704–1713 (2009)
- S. Basu, H.M. Antia, *Mon. Not. R. Astron. Soc.* **287**, 189–198 (1997)
- S. Basu, H.M. Antia, *Astrophys. J. Lett.* **606**, 85–88 (2004)
- S. Basu, H.M. Antia, *Phys. Rep.* **457**, 217–283 (2008)
- S. Basu, J. Christensen-Dalsgaard, *Astron. Astrophys.* **322**, 5–8 (1997)
- S. Basu, W. Däppen, A. Nayfonov, *Astrophys. J.* **518**, 985–993 (1999)
- S. Basu, S. Turck-Chièze, G. Berthomieu, A.S. Brun, T. Corbard, G. Gonczi, J. Christensen-Dalsgaard, J. Provost, S. Thiery, A.H. Gabriel, P. Boumier, *Astrophys. J.* **535**, 1078–1084 (2000)
- S. Basu, W.J. Chaplin, Y. Elsworth, R. New, A.M. Serenelli, G.A. Verner, *Astrophys. J.* **655**, 660–671 (2007)
- S. Basu, W.J. Chaplin, Y. Elsworth, R. New, A.M. Serenelli, *Astrophys. J.* **699**, 1403–1417 (2009)
- S. Basu, A.-M. Broomhall, W.J. Chaplin, Y. Elsworth, *Astrophys. J.* **758**, 43 (2012)
- P.G. Beck, J. Montalbán, T. Kallinger, J. De Ridder, C. Aerts, R.A. García, S. Hekker, M.-A. Dupret, B. Mosser, P. Eggenberger, D. Stello, Y. Elsworth, S. Frandsen, F. Carrier, M. Hillen, M. Gruberbauer, J. Christensen-Dalsgaard, A. Miglio, M. Valentini, T.R. Bedding, H. Kjeldsen, F.R. Girouard, J.R. Hall, K.A. Ibrahim, *Nature* **481**, 55–57 (2012)
- K. Belkacem, *Lecture Notes in Physics*, vol. 832 (Springer, Berlin, 2011)
- K. Belkacem, R. Samadi, M.J. Goupil, M.A. Dupret, A.S. Brun, F. Baudin, *Astron. Astrophys.* **494**, 191–204 (2009)
- C. Blancard, P. Cossé, G. Faussurier, *Astrophys. J.* **745**, 10 (2012)
- E. Böhm-Vitense, *Z. Astrophys.* **46**, 108 (1958)
- A. Bonaca, J.D. Tanner, S. Basu, W.J. Chaplin, T.S. Metcalfe, M.J.P.F.G. Monteiro, J. Ballot, T.R. Bedding, A. Bonanno, A.-M. Broomhall, H. Bruntt, T.L. Campante, J. Christensen-Dalsgaard, E. Corsaro, Y. Elsworth, R.A. García, S. Hekker, C. Karoff, H. Kjeldsen, S. Mathur, C. Régulo, I. Roxburgh, D. Stello, R. Trampedach, T. Barclay, C.J. Burke, D.A. Caldwell, *Astrophys. J. Lett.* **755**, 12 (2012)
- J. Bouvier, *Astron. Astrophys.* **489**, 53–56 (2008)
- J. Braithwaite, *Mon. Not. R. Astron. Soc.* **386**, 1947–1958 (2008)
- J. Braithwaite, *Mon. Not. R. Astron. Soc.* **397**, 763–774 (2009)
- J. Braithwaite, Å. Nordlund, *Astron. Astrophys.* **450**, 1077–1095 (2006)
- J. Braithwaite, H.C. Spruit, *Nature* **431**, 819–821 (2004)
- M.K. Browning, M.S. Miesch, A.S. Brun, J. Toomre, *Astrophys. J. Lett.* **648**, 157–160 (2006)
- A.S. Brun, in *EAS Publications Series*, vol. 44, ed. by H. Wozniak, G. Hensler (2011), pp. 81–95
- A.S. Brun, J.-P. Zahn, *Astron. Astrophys.* **457**, 665–674 (2006)
- A.S. Brun, S. Turck-Chièze, J.P. Zahn, *Astrophys. J.* **525**, 1032–1041 (1999)
- A.S. Brun, M.S. Miesch, J. Toomre, *Astrophys. J.* **742**, 79 (2011)
- E. Caffau, H.-G. Ludwig, P. Bonifacio, R. Faraggiana, M. Steffen, B. Freytag, I. Kamp, T.R. Ayres, *Astron. Astrophys.* **514**, 92 (2010)
- E. Caffau, H.-G. Ludwig, M. Steffen, B. Freytag, P. Bonifacio, *Sol. Phys.* **268**, 255–269 (2011)
- T. Ceillier, P. Eggenberger, R.A. García, S. Mathis, *Astron. Nachr.* **333**, 971 (2012)
- W.J. Chaplin, A.M. Serenelli, S. Basu, Y. Elsworth, R. New, G.A. Verner, *Astrophys. J.* **670**, 872–884 (2007)

- C. Charbonnel, S. Talon, *Science* **309**, 2189–2191 (2005)
- J. Christensen-Dalsgaard, *Rev. Mod. Phys.* **74**, 1073–1129 (2002)
- J. Christensen-Dalsgaard, IFA print (2003). <http://astro.phys.au.dk/~jcd/oscilnotes/>
- J. Christensen-Dalsgaard, W. Dappen, *Astron. Astrophys. Rev.* **4**, 267–361 (1992)
- J. Christensen-Dalsgaard, W. Dappen, S.V. Ajukov, E.R. Anderson, H.M. Antia, S. Basu, V.A. Baturin, G. Berthomieu, B. Chaboyer, S.M. Chitre, A.N. Cox, P. Demarque, J. Donatowicz, W.A. Dziembowski, M. Gabriel, D.O. Gough, D.B. Guenther, J.A. Guzik, J.W. Harvey, F. Hill, G. Houdek, C.A. Iglesias, A.G. Kosovichev, J.W. Leibacher, P. Morel, C.R. Proffitt, J. Provost, J. Reiter, E.J. Rhodes Jr., F.J. Rogers, I.W. Roxburgh, M.J. Thompson, R.K. Ulrich, *Science* **272**, 1286–1292 (1996)
- J. Christensen-Dalsgaard, M.P. Di Mauro, G. Houdek, F. Pijpers, *Astron. Astrophys.* **494**, 205 (2009)
- E.R. Cohen, B.N. Taylor, *Rev. Mod. Phys.* **59**, 1121–1148 (1987)
- S. Couvidat, S. Turck-Chièze, A.G. Kosovichev, *Astrophys. J.* **599**, 1434–1448 (2003)
- A.N. Cox, J.A. Guzik, *Astrophys. J. Lett.* **613**, 169–171 (2004)
- W. Dappen, D.O. Gough, Progress report on helium abundance determination, in *Seismology of the Sun and the Distant Stars; Proceedings of the NATO Advanced Research Workshop*, Cambridge, England, June 17–21, 1985, (A87-20101 07-92) (Reidel, Dordrecht, 1986), pp. 275–280
- W. Dappen, L. Anderson, D. Mihalas, *Astrophys. J.* **319**, 195–206 (1987)
- T. Decressin, S. Mathis, A. Palacios, L. Siess, S. Talon, C. Charbonnel, J.-P. Zahn, *Astron. Astrophys.* **495**, 271–286 (2009)
- S. Deheuvels, R.A. García, W.J. Chaplin, S. Basu, H.M. Antia, T. Appourchaux, O. Benomar, G.R. Davies, Y. Elsworth, L. Gizon, M.J. Goupil, D.R. Reese, C. Regulo, J. Schou, T. Stahn, L. Casagrande, J. Christensen-Dalsgaard, D. Fischer, S. Hekker, H. Kjeldsen, S. Mathur, B. Mosser, M. Pinsonneault, J. Valenti, J.L. Christiansen, K. Kinemuchi, F. Mullally, *Astrophys. J.* **756**, 19 (2012)
- F. Delahaye, M.H. Pinsonneault, *Astrophys. J.* **649**, 529–540 (2006)
- L. Delbouille, G. Roland, L. Neven, *Photometric Atlas of the Solar Spectrum from 3000 to 10000 Å* (Univ. Liege/Obs. Roy. Belg., Liege, 1973) 380 pp.
- L. Delbouille, G. Roland, J. Brault, L. Testerman, *Photometric Atlas of the Solar Spectrum from 1850 to 10000 cm⁻¹* (Kitt Peak Natl. Obs./Univ. Liège, Liege, 1981) 172 pp.
- B. Dintrans, A. Brandenburg, Å. Nordlund, R.F. Stein, *Astron. Astrophys.* **438**, 365–376 (2005)
- J.-F. Donati, J.D. Landstreet, *Annu. Rev. Astron. Astrophys.* **47**, 333–370 (2009)
- V. Duez, S. Mathis, *Astron. Astrophys.* **517**, 58 (2010)
- V. Duez, J. Braithwaite, S. Mathis, *Astrophys. J. Lett.* **724**, 34–38 (2010a)
- V. Duez, S. Mathis, S. Turck-Chièze, *Mon. Not. R. Astron. Soc.* **402**, 271–281 (2010b)
- W.A. Dziembowski, A.A. Pamiatnykh, R. Sienkiewicz, *Mon. Not. R. Astron. Soc.* **249**, 602–605 (1991)
- A. Eff-Darwich, S.G. Korzennik, *Sol. Phys.* **149** (2012)
- P. Eggenberger, A. Maeder, G. Meynet, *Astron. Astrophys.* **440**, 9–12 (2005)
- P. Eggenberger, J. Montalbán, A. Miglio, *Astron. Astrophys.* **544**, 4 (2012)
- P.P. Eggleton, J. Faulkner, B.P. Flannery, *Astron. Astrophys.* **23**, 325 (1973)
- J.R. Elliott, A.G. Kosovichev, *Astrophys. J. Lett.* **500**, 199 (1998)
- Y. Elsworth, R. Howe, G.R. Isaak, C.P. McLeod, R. New, *Nature* **345**, 322–324 (1990)
- D. Fabbian, E. Khomeenko, F. Moreno-Insertis, Å. Nordlund, *Astrophys. J.* **724**, 1536–1541 (2010)
- D. Fabbian, F. Moreno-Insertis, E. Khomeenko, Å. Nordlund, *Astron. Astrophys.* **548**, 35 (2012)
- C. Farner, R. Norton, *A High-Resolution Atlas of the Infrared Spectrum of the Sun and the Earth Atmosphere from Space: A Compilation of ATMOS Spectra of the Region from 650 to 4800 cm⁻¹ (2.3 to 16 μm)*. Vol. I. *The Sun* (Natl. Aeronautics Space Admin., Washington, 1989) 535 pp.
- S.T. Fletcher, A.-M. Broomhall, D. Salabert, S. Basu, W.J. Chaplin, Y. Elsworth, R.A. García, R. New, *Astrophys. J. Lett.* **718**, 19–22 (2010)
- C. Fröhlich, J. Lean, *Geophys. Res. Lett.* **25**, 4377–4380 (1998)
- A.H. Gabriel, G. Grec, J. Charra, J.-M. Robillot, T. Roca Cortés, S. Turck-Chièze, R. Bocchia, P. Boumier, M. Cantin, E. Cespédes, B. Cougrand, J. Crétole, L. Damé, M. Decaudin, P. Delache, N. Denis, R. Duc, H. Dzitko, E. Fossat, J.-J. Fourmond, R.A. García, D. Gough, C. Grivel, J.M. Herreros, H. Lagardère, J.-P. Moalig, P.L. Pallé, N. Pétrou, M. Sanchez, R. Ulrich, H.B. van der Raay, *Sol. Phys.* **162**, 61–99 (1995)
- A.H. Gabriel, F. Baudin, P. Boumier, R.A. García, S. Turck-Chièze, T. Appourchaux, L. Bertello, G. Berthomieu, J. Charra, D.O. Gough, P.L. Pallé, J. Provost, C. Renaud, J.-M. Robillot, T. Roca Cortés, S. Thiery, R.K. Ulrich, *Astron. Astrophys.* **390**, 1119–1131 (2002)
- P. Garaud, J.-D. Garaud, *Mon. Not. R. Astron. Soc.* **391**, 1239–1258 (2008)
- R.A. García, S. Turck-Chièze, S.J. Jiménez-Reyes, J. Ballot, P.L. Pallé, A. Eff-Darwich, S. Mathur, J. Provost, *Science* **316**, 1591 (2007)
- R.A. García, A. Jiménez, S. Mathur, J. Ballot, A. Eff-Darwich, S.J. Jiménez-Reyes, P.L. Pallé, J. Provost, S. Turck-Chièze, *Astron. Nachr.* **329**, 476 (2008)

- R.A. García, D. Salabert, J. Ballot, A. Eff-Darwich, R. Garrido, A. Jiménez, S. Mathis, S. Mathur, A. Moya, P.L. Pallé, C. Régulo, K. Sato, J.C. Suárez, S. Turck-Chièze, *J. Phys. Conf. Ser.* **271**(1), 012046 (2011a)
- R.A. García, D. Salabert, J. Ballot, A. Eff-Darwich, R. Garrido, A. Jiménez, S. Mathis, S. Mathur, A. Moya, P.L. Pallé, C. Régulo, K. Sato, J.C. Suárez, S. Turck-Chièze, *J. Phys. Conf. Ser.* **271**, 012046 (2011b)
- R.J. García Lopez, H.C. Spruit, *Astrophys. J.* **377**, 268–277 (1991)
- B. Gelly, M. Lazrek, G. Grec, A. Ayad, F.X. Schmider, C. Renaud, D. Salabert, E. Fossat, *Astron. Astrophys.* **394**, 285–297 (2002)
- P. Goldreich, P.D. Nicholson, *Astrophys. J.* **342**, 1075–1078 (1989)
- Z. Gong, W. Däppen, L. Zejda, *Astrophys. J.* **546**, 1178–1182 (2001)
- D.O. Gough, M.E. McIntyre, *Nature* **394**, 755–757 (1998)
- N. Grevesse, A. Noels, in *Origin and Evolution of the Elements*, ed. by N. Prantzos, E. Vangioni-Flam, M. Casse (Cambridge University Press, Cambridge, 1993), pp. 15–25, 561 pp.
- N. Grevesse, A.J. Sauval, *Space Sci. Rev.* **85**, 161–174 (1998)
- B. Gustafsson, B. Edvardsson, K. Eriksson, U.G. Jørgensen, Å. Nordlund, B. Plez, *Astron. Astrophys.* **486**, 951–970 (2008)
- J.A. Guzik, K. Mussack, *Astrophys. J.* **713**, 1108–1119 (2010)
- J.A. Guzik, F.J. Swenson, *Astrophys. J.* **491**, 967 (1997). doi:[10.1086/304988](https://doi.org/10.1086/304988)
- J.A. Guzik, L.S. Watson, A.N. Cox, *Astrophys. J.* **627**, 1049–1056 (2005). doi:[10.1086/430438](https://doi.org/10.1086/430438)
- F. Hase, L. Wallace, S.D. McLeod, J.J. Harrison, P.F. Bernath, *J. Quant. Spectrosc. Radiat. Transf.* **111**, 521–528 (2010)
- H. Holweger, E.A. Mueller, *Sol. Phys.* **39**, 19–30 (1974)
- D.G. Hummer, D. Mihalas, *Astrophys. J.* **331**, 794–814 (1988)
- C.A. Iglesias, F.J. Rogers, *Astrophys. J.* **464**, 943 (1996)
- S.D. Kawaler, *Astrophys. J.* **333**, 236–247 (1988)
- E.-J. Kim, K.B. MacGregor, *Astrophys. J.* **588**, 645–654 (2003)
- A.G. Kosovichev, J. Christensen-Dalsgaard, W. Daepfen, W.A. Dziembowski, D.O. Gough, M.J. Thompson, *Mon. Not. R. Astron. Soc.* **259**, 536–558 (1992)
- C.J. Lada, *IAU Symposium*, vol. 115 (1987)
- D. Lecoanet, E. Quataert, *Mon. Not. R. Astron. Soc.* **430**, 2363 (2013). doi:[10.1093/mnras/stt055](https://doi.org/10.1093/mnras/stt055)
- L.H. Li, F.J. Robinson, P. Demarque, S. Sofia, D.B. Guenther, *Astrophys. J.* **567**, 1192–1201 (2002)
- K.G. Libbrecht, M.F. Woodard, *Nature* **345**, 779–782 (1990)
- K. Lodders, Solar system abundances of the elements, in *Principles and Perspectives in Cosmochemistry, Astrophysics and Space Science Proceedings* (Springer, Berlin, 2010), p. 379. ISBN 978-3-642-10351-3, doi:[10.1007/978-3-642-10352-0_8](https://doi.org/10.1007/978-3-642-10352-0_8)
- I. Lopes, S. Turck-Chièze, *Astrophys. J.* **765**(1), 14–23 (2013)
- A. Maeder, *Physics, Formation and Evolution of Rotating Stars*. *Astron. Astrophys. Library* (Springer, Berlin, 2009). doi:[10.1007/978-3-540-76949-1](https://doi.org/10.1007/978-3-540-76949-1)
- A. Maeder, J.-P. Zahn, *Astron. Astrophys.* **334**, 1000–1006 (1998)
- J.P. Marques, M.J. Goupil, Y. Lebreton, S. Talon, A. Palacios, K. Belkacem, R.-M. Ouazzani, B. Mosser, A. Moya, P. Morel, B. Pichon, S. Mathis, J.-P. Zahn, S. Turck-Chièze, P.A.P. Nghiem, *Astron. Astrophys.* **549**, 74 (2013)
- S. Mathis, *Astron. Astrophys.* **506**, 811–828 (2009)
- S. Mathis, in *Lecture Notes in Physics*, vol. 865, ed. by M. Goupil, K. Belkacem, C. Neiner, F. Lignières, J.J. Green (Springer, Berlin, 2013), p. 23
- S. Mathis, N. de Brye, *Astron. Astrophys.* **526**, 65 (2011)
- S. Mathis, N. de Brye, *Astron. Astrophys.* **540**, 37 (2012)
- S. Mathis, J.-P. Zahn, *Astron. Astrophys.* **425**, 229–242 (2004)
- S. Mathis, J.-P. Zahn, *Astron. Astrophys.* **440**, 653–666 (2005)
- S. Mathis, S. Talon, F.-P. Pantillon, J.-P. Zahn, *Sol. Phys.* **251**, 101–118 (2008)
- S. Matt, R.E. Pudritz, *Astrophys. J. Lett.* **632**, 135–138 (2005)
- S.P. Matt, K.B. MacGregor, M.H. Pinsonneault, T.P. Greene, *Astrophys. J. Lett.* **754**, 26 (2012)
- L. Mestel, in *IAU Symposium*, vol. 22, ed. by R. Lust (1965), p. 420
- L. Mestel, R.J. Tayler, D.L. Moss, *Mon. Not. R. Astron. Soc.* **231**, 873–885 (1988)
- D. Mihalas, W. Däppen, D.G. Hummer, *Astrophys. J.* **331**, 815–825 (1988)
- D. Moss, *Mon. Not. R. Astron. Soc.* **257**, 593–601 (1992)
- B. Mosser, M.J. Goupil, K. Belkacem, J.P. Marques, P.G. Beck, S. Bloemen, J. De Ridder, C. Barban, S. Deheuvels, Y. Elsworth, S. Hekker, T. Kallinger, R.M. Ouazzani, M. Pinsonneault, R. Samadi, D. Stello, R.A. García, T.C. Klaus, J. Li, S. Mathur, R.L. Morris, *Astron. Astrophys.* **548**, 10 (2012)
- H. Neckel, D. Labs, *Sol. Phys.* **90**, 205–258 (1984)
- Å. Nordlund, R.F. Stein, M. Asplund, *Living Rev. Sol. Phys.* **6**, 2 (2009)
- G.I. Ogilvie, D.N.C. Lin, *Astrophys. J.* **661**, 1180–1191 (2007)

- L. Piau, R. Collet, R.F. Stein, R. Trampedach, P. Morel, S. Turck-Chièze, *Mon. Not. R. Astron. Soc.* **437**, 164 (2014). doi:[10.1093/mnras/stt1866](https://doi.org/10.1093/mnras/stt1866)
- M.H. Pinsonneault, S.D. Kawaler, S. Sofia, P. Demarque, *Astrophys. J.* **338**, 424–452 (1989)
- R.F. Pinto, A.S. Brun, L. Jouve, R. Grappin, *Astrophys. J.* **737**, 72 (2011)
- F. Remus, S. Mathis, J.-P. Zahn, *Astron. Astrophys.* **544**, 132 (2012)
- O. Richard, S. Vauclair, C. Charbonnel, W.A. Dziembowski, *Astron. Astrophys.* **312**, 1000–1011 (1996)
- O. Richard, W.A. Dziembowski, R. Sienkiewicz, P.R. Goode, *Astron. Astrophys.* **338**, 756–760 (1998)
- M. Rieutord, *Astron. Astrophys.* **451**, 1025–1036 (2006)
- J. Robrade, J.H.M.M. Schmitt, F. Favata, *Astron. Astrophys.* **486**, 995–1002 (2008)
- T.M. Rogers, G.A. Glatzmaier, *Mon. Not. R. Astron. Soc.* **364**, 1135–1146 (2005)
- T.M. Rogers, K.B. MacGregor, *Mon. Not. R. Astron. Soc.* **410**, 946–962 (2011)
- F.J. Rogers, A. Nayfonov, *Astrophys. J.* **576**, 1064–1074 (2002)
- F.J. Rogers, F.J. Swenson, C.A. Iglesias, *Astrophys. J.* **456**, 902 (1996)
- C.S. Rosenthal, J. Christensen-Dalsgaard, Å. Nordlund, R.F. Stein, R. Trampedach, *Astron. Astrophys.* **351**, 689–700 (1999)
- G. Rudiger, L.L. Kitchatinov, *Astron. Nachr.* **318**, 273 (1997)
- G. Rüdiger, L.L. Kitchatinov, D. Elstner, *Mon. Not. R. Astron. Soc.* **425**, 2267–2276 (2012)
- D. Salabert, R.A. García, P.L. Pallé, S.J. Jiménez-Reyes, *Astron. Astrophys. Lett.* **504**, 1–4 (2009)
- E. Schatzman, *Astron. Astrophys.* **279**, 431–446 (1993a)
- E. Schatzman, *Astron. Astrophys.* **271**, 29 (1993b)
- P.H. Scherrer, R.S. Bogart, R.I. Bush, J.T. Hoeksema, A.G. Kosovichev, J. Schou, W. Rosenberg, L. Springer, T.D. Tarbell, A. Title, C.J. Wolfson, I. Zayer, MDI Engineering Team, *Sol. Phys.* **162**, 129–188 (1995)
- J.T. Schmelz, K. Nasraoui, J.K. Roames, L.A. Lippner, J.W. Garst, *Astrophys. J. Lett.* **634**, 197–200 (2005)
- J. Schou, H.M. Antia, S. Basu, R.S. Bogart, R.I. Bush, S.M. Chitre, J. Christensen-Dalsgaard, M.P. di Mauro, W.A. Dziembowski, A. Eff-Darwich, D.O. Gough, D.A. Haber, J.T. Hoeksema, R. Howe, S.G. Korzenik, A.G. Kosovichev, R.M. Larsen, F.P. Pijpers, P.H. Scherrer, T. Sekii, T.D. Tarbell, A.M. Title, M.J. Thompson, J. Toomre, *Astrophys. J.* **505**, 390–417 (1998)
- H. Schwabe, *Astron. Nachr.* **21**(495), 233–236 (1844)
- A.M. Serenelli, S. Basu, *Astrophys. J.* **719**, 865–872 (2010)
- R. Simoniello, K. Jain, S.C. Tripathy, S. Turck-Chièze, C. Baldner, W. Finsterle, F. Hill, M. Roth, *Astrophys. J.* (2013). doi:[10.1088/0004-637X/765/2/100](https://doi.org/10.1088/0004-637X/765/2/100)
- F. Spada, A.C. Lanzafame, A.F. Lanza, *Mon. Not. R. Astron. Soc.*, **404**, 641–660 (2010)
- E.A. Spiegel, J.-P. Zahn, *Astron. Astrophys.* **265**, 106–114 (1992)
- H.C. Spruit, *Astron. Astrophys.* **349**, 189–202 (1999)
- H.C. Spruit, *Astron. Astrophys.* **381**, 923–932 (2002)
- R.F. Stein, Å. Nordlund, *Astrophys. J.* **499**, 914 (1998)
- A. Strugarek, A.S. Brun, J.-P. Zahn, *Astron. Astrophys.* **532**, 34 (2011a)
- A. Strugarek, A.S. Brun, J.-P. Zahn, *Astron. Nachr.* **332**, 891 (2011b)
- M. Takata, H. Shibahashi, in *IAU Symposium*, vol. 185, ed. by F.-L. Deubner, J. Christensen-Dalsgaard, D. Kurtz, (1998), p. 21
- S. Talon, C. Charbonnel, *Astron. Astrophys.* **440**, 981–994 (2005)
- R.J. Tayler, *Mon. Not. R. Astron. Soc.* **161**, 365 (1973)
- I. Thaler, Private communication, 2012
- S. Turck-Chièze, S. Couvidat, *Rep. Prog. Phys.* **74**(8), 086901 (2011)
- S. Turck-Chièze, P. Lambert, *Adv. Space Res.* **40**, 907–914 (2007)
- S. Turck-Chièze, I. Lopes, *Astrophys. J.* **408**, 347–367 (1993)
- S. Turck-Chièze, I. Lopes, *Res. Astron. Astrophys.* **12**, 1107–1138 (2012)
- S. Turck-Chièze, The OPAC consortium. *High Energy Density Phys.* **9**, 473 (2013). doi:[10.1016/j.hedp.2013.04.004](https://doi.org/10.1016/j.hedp.2013.04.004)
- S. Turck-Chièze, W. Däppen, E. Fossat, J. Provost, E. Schatzman, D. Vignaud, *Phys. Rep.* **230**, 57–235 (1993)
- S. Turck-Chièze, S. Couvidat, A.G. Kosovichev, A.H. Gabriel, G. Berthomieu, A.S. Brun, J. Christensen-Dalsgaard, R.A. García, D.O. Gough, J. Provost, T. Roca-Cortés, I.W. Roxburgh, R.K. Ulrich, *Astrophys. J. Lett.* **555**, 69–73 (2001)
- S. Turck-Chièze, S. Couvidat, L. Piau, J. Ferguson, P. Lambert, J. Ballot, R.A. García, P. Nghiem, *Phys. Rev. Lett.* **93**(21), 211102 (2004a)
- S. Turck-Chièze, R.A. García, S. Couvidat, R.K. Ulrich, L. Bertello, F. Varadi, A.G. Kosovichev, A.H. Gabriel, G. Berthomieu, A.S. Brun, I. Lopes, P. Pallé, J. Provost, J.M. Robillot, T. Roca Cortés, *Astrophys. J.* **604**, 455–468 (2004b)
- S. Turck-Chièze, F. Delahaye, D. Gilles, G. Loisel, L. Piau, *High Energy Density Phys.* **5**, 132–138 (2009)
- S. Turck-Chièze, A. Palacios, J.P. Marques, P.A.P. Nghiem, *Astrophys. J.* **715**, 1539–1555 (2010a)
- S. Turck-Chièze, A. Palacios, J.P. Marques, P.A.P. Nghiem, *Astrophys. J.* **715**, 1539–1555 (2010b)

- S. Turck-Chièze, L. Piau, S. Couvidat, *Astrophys. J. Lett.* **731**, 29 (2011)
- S. Turck-Chièze, R.A. García, I. Lopes, J. Ballot, S. Couvidat, S. Mathur, D. Salabert, J. Silk, *Astrophys. J. Lett.* **746**, 12–16 (2012)
- S.V. Vorontsov, V.A. Baturin, S.V. Ayukov, V.K. Gryaznov, *Mon. Not. R. Astron. Soc.* **430**, 1636–1652 (2013). doi:[10.1093/mnras/sts701](https://doi.org/10.1093/mnras/sts701)
- T.S. Wood, J.O. McCaslin, P. Garaud, *Astrophys. J.* **738**, 47 (2011)
- P.R. Young, *Astron. Astrophys.* **444**, 45–48 (2005)
- J.P. Zahn, *Ann. Astrophys.* **29**, 489 (1966)
- J.-P. Zahn, *Astron. Astrophys.* **41**, 329–344 (1975)
- J.-P. Zahn, *Astron. Astrophys.* **252**, 179–188 (1991)
- J.-P. Zahn, *Astron. Astrophys.* **265**, 115–132 (1992)
- J.-P. Zahn, L. Bouchet, *Astron. Astrophys.* **223**, 112–118 (1989)
- J.-P. Zahn, S. Talon, J. Matias, *Astron. Astrophys.* **322**, 320–328 (1997)
- J.-P. Zahn, A.S. Brun, S. Mathis, *Astron. Astrophys.* **474**, 145–154 (2007)
- C. Zanni, J. Ferreira, *Astron. Astrophys.* **550**, 99 (2013)
- C. Zhang, L. Deng, D. Xiong, J. Christensen-Dalsgaard, *Astrophys. J. Lett.* **759**, 14 (2012)